Low post-glacial rebound rates in the Weddell Sea due to Late Holocene ice-sheet readvance

Sarah L.Bradley[1,2*], Richard C.A. Hindmarsh[1], Pippa.L.Whitehouse[3], Michael J.Bentley[3], Matt A. King[4]

[1] British Antarctic Survey, Cambridge, UK
[2] Institute for Marine and Atmospheric research, Utrecht University, Utrecht, Netherlands
[3] Department of Geography, Durham University, Durham, UK.
[4] Surveying and Spatial Sciences, School of Land and Food, University of Tasmania, Hobart, Australia.

*****Corresponding author. E-mail: d80ngv@gmail.com

Abstract

Many ice-sheet reconstructions assume monotonic Holocene retreat for the West Antarctic Ice Sheet, but an increasing number of glaciological observations infer that some portions of the ice sheet may be readvancing, following retreat behind the present-day margin. A readvance in the Weddell Sea region can reconcile two outstanding problems: (i) the present-day widespread occurrence of seemingly stable ice streams grounded on beds that deepen inland; and (ii) the inability of models of glacial isostatic adjustment to match present-day uplift rates. By combining a suite of ice loading histories that include a readvance with a model of glacial isostatic adjustment we report substantial improvements to predictions of present-day uplift rates, including reconciling one problematic observation of land sinking. We suggest retreat behind present grounding lines occurred when the bed was lower, and isostatic recovery has since led to shallowing, ice sheet re-grounding and readvance. The paradoxical existence of grounding lines in apparently unstable configurations on reverse bed slopes may be resolved by invoking the process of unstable advance, in accordance with our load modelling.

1. Introduction

The Weddell Sea sector remains one of the most poorly studied regions of the Antarctic Ice Sheet (AIS), and there are still many gaps in our understanding of past and present grounding-line behaviour in this region. Ice sheet grounding lines located in regions where the bed deepens inland (“reverse bed slopes”) are generally inherently unstable (Schoof, 2007). Such configurations are common along the Weddell Sea sector of the West Antarctic Ice Sheet (WAIS), leading to concerns that small perturbations may produce wide-spread ice sheet retreat and sea-level rise (Joughin and Alley, 2011). The potential rate of operation of this instability is exacerbated by the relatively low ice-thickness gradients upstream of the grounding line (Ross et al., 2012). It remains unclear how the ice sheet could have evolved into an apparently unstable state from a thicker and more extensive Last Glacial Maximum (LGM) configuration (Bentley et al., 2010). It may be that the grounding line is unstable but is only retreating slowly or, it may be that a combination of the buttressing effect of the Filchner-Ronne Ice Shelf (FRIS) (Gudmundsson, 2013) and local perturbations to sea surface height and bedrock elevation due to ice load changes (Gomez et al., 2013) act to stabilize the grounding line. Alternatively, the controls on grounding line motion may have evolved such that the grounding-line is unstable, but now advancing subsequent to post-LGM retreat.

Little is known of changes within the Weddell Sea area of WAIS over recent decades to millenia (Bentley et al., 2010; Le Brocq et al., 2011; Whitehouse et al., 2012a; Hillenbrand et al., 2013); some large scale ice sheet reconstructions assume deglaciation terminated between 4 and 2 kyr (before present, BP) (Peltier, 2004: Whitehouse et al., 2012a) while others assume monotonic thinning to 1 kyr BP (Ivins et al., 2013). A previous investigation (Bindschadler et al., 1990) found evidence for re-grounding of the ice sheet in the Siple Coast region within the past 1000 years. A more recent glaciological investigation (Siegert et al., 2013) used radar-echo sounding data to investigate the englacial layering and surface forms within the slow-flowing Bungenstock Ice Rise (BIR), which seperates the fast-flowing Institude and Möller ice streams (IIS and MIS, respectively) within the Weddell Sea embayment (Fig.1). That study found evidence for Late Holocene (at the earliest 4 kyr BP) flow reorganisation across the BIR and proposed two hypotheses to explain this change (see Fig.5 and Table 1 in Siegert et al., 2013); (i) ice-stream flow was reorganized without significant ice volume change or movement of the grounding line position or (ii) the grounding line retreated inland of the present-day position, with readvance of the ice sheet to its present-day configuration driven by bedrock uplift and subsequent ice sheet re-grounding.

Importantly, the two hypotheses potentially produce distinctly different patterns of present-day Glacial Isostatic Adjustment (GIA) (Ivins et al., 2000) - the ongoing solid Earth response to changes in ice-ocean surface loading – and consequently have different implications for present-day ice sheet stability. Additionally, the studies of Bindschadler et al., (1990) and Siegert et al., (2013) imply that the assumption of a simple monotonic Late Holocene deglaciation history of the WAIS needs to be re-evaluated.

Several GIA models for Antarctica have been developed (Whitehouse et al., 2012b; Gomez et al., 2013; Ivins et al., 2013; Argus et al., 2014) with the objective of simultaneously constraining the spatial and temporal history of the AIS and the rheological properties of the solid Earth. There are many differences in the inferred maximum size and deglaciation histories of the ice sheet (Peltier, 2004; Whitehouse et al., 2012a; Gomez et al., 2013; Ivins et al., 2013), with still very little known about the late Holocene history in the Weddell Sea - a period that will strongly influence the present-day GIA signal**.** This uncertainty is primarily due to the paucity of observations that can constrain the ice-loading history (Whitehouse et al., 2012a; Hillenbrand et al., 2013).

Here we investigate whether the post-LGM shallowing of the grounding line and a consequent GIA-induced readvance can explain the glaciological data (Siegert et al., 2013) and the absence of rapid retreat (Joughin and Bamber, 2005; Lambrecht et al., 2007) within this region. We develop a suite of revised Late Holocene deglaciation patterns to explore the two hypothesis proposed by Siegert et al., (2013). These revised ice-loading histories simulate thinning and re-thickening without grounding line migration, or an ice margin that undergoes an extended retreat behind the present-day grounding line, a stillstand and subsequent readvance to the present-day extent. By combining each of these simulations with a GIA model, predictions of the present-day uplift rates can be compared with those measured by Global Positioning System (GPS) at sites around the southern edge of the FRIS to assess the plausibility of the various ice-loading simulations.

2. Method

2.1 Glacial Isostatic Adjustment model

The GIA model used in this study to generate predictions of solid Earth deformation and present-day uplift rates adopts a spectral technique (Mitrovica et al., 1994) which has been extended to take into account perturbations in Earth's rotation (Mitrovica et al., 2001). The three model components (Earth model, sea level solver and ice model) are outlined in greater detail below.

The Earth model considers a compressible, spherically symmetric, self-gravitating Maxwell viscoelastic body, where the depth-dependence of the elastic parameters and density is taken from PREM (Dziewonski and Anderson, 1981) at a resolution of 10 km in the crust and 25 km in the mantle. The viscosity structure is parameterized into three main layers: a high viscosity (10^{43} Pa s) upper layer to approximate an elastic lithosphere, an upper mantle region extending from beneath the lithosphere to the 660 km discontinuity and a lower mantle region extending from there to the core-mantle boundary. The thickness of the lithosphere and the viscosity of the upper and lower mantle are user-defined parameters. It has been suggested that there is considerable lateral variability beneath the Antarctic continent (Morelli and Danesi, 2004; Chaput et al., 2014), from the relatively thin lithosphere and low viscosity mantle believed appropriate for the West Antarctic rift system to the thicker lithosphere and higher viscosity mantle of the craton below East Antarctica. Consequently, there have been considerable differences in the Earth model used in previous Antarctic GIA modelling studies (Peltier, 2004; Whitehouse et al., 2012b; Ivins et al., 2013). For the main basis of the study, the optimum Earth model of Whitehouse et al., (2012b) was adopted, which has a lithospheric thickness of 120 km, an upper mantle viscosity of 1×10^{21} Pa s and a lower mantle viscosity of 1×10^{22} Pa s. However, to investigate model sensitivity, present-day uplift rates were generated using seven different Earth models (see Table S2 and Section 3.2). This spread of Earth models explores the minimum-maximum limits of lithospheric thickness and upper and lower mantle viscosities inferred from a range of GIA studies (Lambeck et al., 1998; Mitrovica and Forte, 2004; Steffen and Kaufmann, 2005; Whitehouse et al., 2012b; Ivins et al., 2013).

A sea level solver is used to solve the generalized sea-level equation (Milne and Mitrovica, 1998; Kendall et al., 2005). It accounts for time-varying shoreline migration, changes in sea level in regions of ablating marine-based ice and the influence of GIA perturbations upon the Earth's rotation vector (Milne and Mitrovica, 1998; Mitrovica et al., 2005). The sea level solver ignores ice loads that cannot ground for a given water depth, instead replacing them with water loads.

2.2 Ice-loading models

As a basis for our experiments, we adopt the W12 ice-loading model (Whitehouse et al., 2012a), the development of which is outlined in greater detail below (Section 2.2.1). To generate the revised ice-loading simulations discussed in Sections 2.2.2 and 2.2.3 the ice thickness distribution in the W12 model was heuristically altered; unlike W12, our revised deglaciation patterns for the AIS were not produced using the output from an ice sheet model.

The exact timing and nature of the post-LGM retreat of the grounding line in the Weddell Sea sector of the W12 model is not very well constrained, owing to the paucity of observations relating to the spatial and temporal history of the ice sheet within this region (see Fig. 1 in Whitehouse et al., 2012a & Hillenbrand et al., 2013). Consequently, the evolution of the W12 grounding line within the Weddell Sea sector was simply tuned to fit onshore ice sheet palaeo-elevation data; its position is not constrained by any offshore data. Importantly, palaeo-elevation data only define the envelope of maximum ice-surface elevation achieved through time, and current data cannot exclude lowering and subsequent recovery. Given this, a series of revised LGM–early Holocene (10 kyr BP) ice-loading simulations were developed (Section 2.2.2) to investigate the sensitivity of the modelled uplift rates to the relatively unconstrained deglaciation history immediately following the LGM. Section 2.2.3 describes the generation of the ensemble of Holocene ice-loading simulations that represent the hypothesized Late Holocene deglaciation-readvance patterns in the Weddell Sea sector.

2.2.1 The W12 ice model

The AIS component of the W12 model was developed using the GLIMMER numerical ice-sheet model (Rutt et al., 2009), and the reconstruction was tuned to fit an extensive database of geological and glaciological evidence relating to past spatial and temporal changes in ice thickness and grounding-line extent. This AIS model was then combined with the ICE-5G v1.2 (Peltier, 2004) global ice model, which was used to define the history of all other ice sheets (such as Greenland and Laurentide). The ICE-5G model was chosen as it is the most coherent global model currently available, but we note that it is over a decade old and numerous deficiencies exist (e.g., Argus and Peltier, 2010); while a very recent revision has been made to the Antarctic component (Argus et al., 2014) it is not yet available. Within the Weddell Sea, the W12 ice sheet is modelled to undergo steady retreat from its maximum extent at the LGM (~ 20 kyr BP, see Fig. 7 of Whitehouse et al., 2012a), where it is grounded out to the continental shelf break, reaching the edge of the Henry and Korff Ice Rises (HIR, KIR see Fig.1A) by 10 kyr BP and reaching present-day extent by 2 kyr BP. To the west and east of Berkner Island (see Fig. 1), in zones of simulated fast-flowing ice (see Fig. 2 of Whitehouse et al., 2012a), the ice margin retreats faster, reaching ~ 80°S by 15 kyr BP. Whitehouse et al., (2012b) considered some Late Holocene (1 kyr BP to present) variations to the W12 model, but only within the Antarctic Peninsula; we do not consider these variations here. Fig. S1 provides an example of the surface elevation in the W12 model at various time slices from 5 kyr BP to present day.

We now describe three groups of simulations: the first explores the effect of LGM thickness and deglaciation speed; the second explores the style of Holocene behaviour to test the two hypotheses in Siegert et al., (2013); and a third group explores the detailed pattern of one of these hypotheses involving retreat and readvance.

2.2.2: Development of revised LGM–early Holocene ice-loading simulations

Whitehouse et al., (2012b) investigated the sensitivity of present-day uplift rates to the timing and rate of deglaciation prior to 5 kyr BP and concluded that there was a negligible~ (0.5 mm/yr) difference between a range simulations. However, the study did not explore in detail the retreat pattern in the Weddell Sea region. In consequence, three revised LGM–early Holocene (10 kyr BP) ice-loading simulations were generated; two explore the sensitivity to the timing of the retreat back from the continental shelf break (LGMA and LGMB) and one (LGMC) investigates the sensitivity to the maximum LGM thickness of the ice sheet. In all three models the ice-loading history from 10 kyr BP to present was unaltered within W12. This cut-off time was chosen because from 10 kyr BP to present there is only a minor retreat of the grounding line back from the HIR and KIR to the present-day extent within the W12 model (see Fig. 7e and Fig. 7f of Whitehouse et al., 2012a).

In models LGMA and LGMB the timing of retreat back from the continental shelf break was altered to yield a slower retreat in LGMA, and a more rapid retreat in LGMB, with the maximum LGM thickness of the ice sheet unchanged from W12. In LGMA, the retreat of the lobe of grounded ice that extended into the central Weddell Sea during the LGM (as shown in Fig. 7b of Whitehouse et al., 2012a) is slowed. This lobe is simulated to remain grounded until 10 kyr BP, undergoing only gradual thinning and minor lateral retreat in comparison with the rapid thinning and extensive lateral retreat seen in the W12 model. Additionally, retreat in the regions of simulated fast-flowing ice to the east and west of Berkner Island (see Fig. 2 of Whitehouse et al., 2012a) is delayed in LGMA, so that grounded ice is simulated to remain across the region currently covered by the Filchner-Ronne Ice Shelf (FRIS) until 10 kyr BP, compared with 15 kyr BP in W12. In LGMB the ice is simulated to retreat back to the HIR and KIR by 15 kyr BP, compared with 10 kyr BP in W12. In the LGMC simulation, the central lobe of grounded ice extending out into the Weddell Sea at the LGM (see Fig. 7b of Whitehouse et al., 2012a) was thickened to over 3000 m (compared with 1000-1500 m in W12). From this revised LGM configuration, the ice was simulated to undergo a steady linear retreat back to the W12 10 kyr BP ice extent.

2.2.3: Development of revised Late Holocene ice-loading simulations

We now describe our modelling procedures aimed at improving the fit of predicted and observed uplift rates. The W12 ice-loading model is adapted to generate an ensemble of Holocene ice-loading simulations representing hypothesized Late Holocene deglaciation patterns in the Weddell Sea. In all these revised ice-loading simulations only the post-6 kyr BP ice extent within the Weddell Sea component of W12 is altered (highlighted by the dashed black line in Fig.1B); the evolution of the rest of the AIS and all other global ice sheets remains the same.

In our experiments we explore the sensitivity of present-day uplift rates to both the configuration and timing of Late Holocene ice loading in the Weddell Sea region. First we describe three ‘minimum’ configurations of the Late Holocene ice sheet, which were generated to explore the two hypotheses proposed by Siegert et al., (2013).
In all three of these simulations, described below, the same timing (kyr BP) and duration (kyr) for the retreat or thinning and subsequent readvance or re-thickening of the ice margin was adopted. From a starting configuration of the W12 model at 6 kyr BP, the ice margin is simulated to undergo either thinning (W12_Thin, Fig. 2) or an extended retreat (W12_Min (Fig. 3) and W12_Max (Fig. S4)), reaching the minimum configuration (see Fig. S2d, Fig. S3d and Fig. S4d, respectively, in supplementary materials) by 3 kyr BP. Between 3 kyr BP and 2 kyr BP a stillstand is simulated, following which the ice margin is simulated to undergo a re-advance (W12_Min and W12_Max) or re-thickening (W12_Thin), reaching the present-day extent by 0 kyr BP.

The W12_Thin simulation (Fig. 2) was created to explore the hypothesis that ice-stream flow was reorganized during the Late Holocene without significant ice volume change or movement of the grounding line position (Siegert et al., 2013). In this simulation there is no lateral retreat of the ice margin behind the present-day location, instead the ice thickness across the BIR is altered so that the surface elevation is the same as the neighbouring IIS and MIS (compare Fig.1B to Fig. 2B). The magnitude of this thinning is such that ice is still lightly grounded across the BIR.

The two simulations, W12_Min (Fig. 3 and Fig. S3) and W12_Max (Fig. S4), were generated to investigate the second hypothesis proposed by Siegert et al., (2013); that the grounding line retreated inland of its present-day position at some point during the Holocene, and this was followed by readvance to the present-day situation. In testing this hypothesis we assume that the ice margin only retreated in regions where the ice sheet is grounded below sea level, and that there would have been additional ice-sheet thinning immediately upstream of the revised ice margin (see Fig. S3 and S4). Since there are few constraints on the total extent of retreat we consider two situations: In the W12_Min case the ice margin retreats behind the present-day grounding lines of the Evans Ice Stream (EIS), IIS and MIS, and across the BIR, but much of the Robin subglacial basin remains ice covered (see Fig. 1A and Fig. 3). In the W12_Max case both the Robin subglacial basin and the BIR are completely deglaciated (see Fig. S4d). The extent of retreat is in practice mainly constrained by considering the impact of each scenario on modelled uplift rates at site 3, the most interior of the GPS sites.

Using the W12_Min configuration as a template (see Fig. 3) we also varied the timing (kyr BP) and duration (kyr) of the retreat and subsequent readvance to produce a further 23 Holocene ice-loading simulations (Table 1). In each case, the ice margin is simulated to undergo an extended steady retreat (see Fig. 3), a stillstand, and subsequent readvance to present-day extent (see Fig. 1B). Fig. S3 provides an example of the spatial extent of the ice sheet at various time slices during the retreat-stillstand-readvance cycle. This simulated retreat-readvance involves an average change in ice mass of 2.7×10^5 Gt (but zero net change in volume between the start and final configuration).

In each of these 23 ice-loading simulations the ice sheet is already retreating prior to the onset of the extended retreat. For our purposes the timing of this onset simply refers to the point at which the spatial extent and rate of retreat is altered from the W12 model, and the new target for ice sheet retreat is the reduced extent shown on Fig. 3. In Table 1, the ice-loading simulations are divided into three groups depending on the timing of the onset of the extended retreat; 6 kyr BP (W12_6*), 5 kyr BP (W12_5*) and 4 kyr BP (W12_4*).

There are three simulations with no stillstand where the ice margins experience a linear retreat and instantly commence a readvance, both over 2 kyr. Further simulations explored the sensitivity of predictions to (i) the initiation (6 kyr BP, 5 kyr BP and 4 kyr BP) and duration (3 kyr, 2 kyr and 1 kyr) of the extended retreat; (ii) the duration of the stillstand (1 kyr, 2 kyr and 3 kyr); and (iii) the duration of the readvance (3, 2 or 1 kyr) and the timing of the end of the readvance (2 kyr BP, 1 kyr BP and 0 kyr BP). Where a stillstand is incorporated, the ice margin is maintained at the maximum retreated extent for the duration (Fig. 3, Fig. S3 and Fig. S4).

These adaptations sample a simple but reasonable distribution of non-monotonic retreat scenarios. Such long-term average retreat rates of 100 m a year, comparative to the retreat rates simulated here, have been inferred for the Ross Sea (Conway et al., 1999), while modelling ((Pollard and DeConto, 2009); see their SOM, Video 1) indicates that retreats and readvances at these rates are physically reasonable.

2.3 GPS Data

A recently-compiled set of Global Positioning System (GPS)-observed bedrock uplift rates (Thomas et al., 2011) at seven sites around the FRIS (see Fig. 1A and Table S1) are used to assess the plausibility of the modelled present-day uplift rates that are derived using the suite of ice-loading/Earth model combinations described above within the GIA model. We adopt the GPS velocities of Thomas et al., (2011) after applying their tabulated elastic correction that is based on ICESat altimetry (Thomas et al., 2011 SOM), and these are repeated in our

Table S1. To reflect the uncertainty in this correction we also list GPS velocities corrected using the alternate elastic model of Thomas et al., (2011).

At six of the seven GPS sites (Fig. 4), the elastic-corrected solid Earth is uplifting at between 2.1 mm/yr (± 1.0 mm/yr; all uncertainties are 1-sigma) and 4.5 mm/yr (±2.6 mm/yr); this magnitude of solid Earth motion is typical following the deglaciation of an ice sheet (Milne et al., 2004) although these rates are noticeably smaller than many current GIA model predictions for Antarctica (Peltier, 2004; Whitehouse et al., 2012b). At site 4 (Fig. 4) the solid Earth is either subsiding or the uplift rate is near-zero (-2.5 mm/yr ± 2.4 mm/yr), in marked contrast to nearby uplifting sites. The three studies that have analyzed the data at site 4 have obtained similar rates (-4.4±2.3 mm/yr (Bevis et al., 2009); -4.3± 3.0 mm/yr (Argus et al., 2011) and -2.5± 2.4 mm/yr (Thomas et al., 2011) after applying a consistent elastic correction; all uncertainties 1-sigma). We also note that applying the alternative elastic correction (Table S1) results in greater subsidence at site 4. Given the independent techniques and reference frames used, and considering quoted uncertainties, we regard this as a strong indication of near-zero or negative uplift at this site.

3. Preliminary Results and Sensitivity testing

Using the GIA model, predictions of present-day uplift rates, for each of the ice-loading simulations, were generated for each GPS site. To assess the degree of fit between modelled and observed (elastic-corrected) uplift rates at each GPS site (*i*) the weighted root mean square error (WRMSE) is calculated:

$$WRMSE = \sqrt{\frac{\sum (o_i - \rho_i)^2 \omega_i}{\sum \omega_i}} \qquad \text{where } \omega_i = \frac{1}{(\sigma_i)^2}$$

o_i and ρ_i are the observed and modelled uplift rate, respectively, and σ_i is the 1-sigma error at each GPS site.

3.1: Starting Ice model

The original W12 model over-predicts the observed uplift rate at six of the seven GPS sites (Whitehouse et al., 2012b), with the predictions biased high with a mean bias of 3.4 mm/yr and a WRMSE of 3.3 mm/yr (see Fig. 4 and Table 1). Notably, the W12 model does not capture the spatial variation in the observed signal, specifically the near-zero/negative uplift at site 4.

3.2: Sensitivity of the modelled present-day uplift rates to the adopted input Earth model

Here we investigate whether W12's over-prediction of uplift (Fig. 4) can be reduced and whether the distinct spatial variation (notably the subsidence at site 4) can be reproduced with a change in just the adopted Earth model parameters. Modelled present-day uplift rates for seven Earth models (Table S2) are compared with the observed (elastic-corrected) rates at the seven sites in Fig. 5A.

The modelled uplift rates are relatively insensitive to changes in the lithospheric thickness, with a maximum difference of only 1.5 mm/yr (between models that adopt a 120 km and a 71 km lithospheric thickness in Fig. 5A). Adopting a weaker lower mantle viscosity (10^{21} Pa s, model 12011 in Fig. 5A) or a stronger upper mantle viscosity (5×10^{21} Pa s, model 120510 in Fig. 5A) resolves the over-prediction at some sites (site 6, 7 or 3) and nearly captures the observed rates (within the 1-sigma uncertainty) at sites 1, 2, and 5, but still significantly over-predicts the near-zero/negative rate at site 4 (by 1.8 mm/yr and 4.2 mm/yr, respectively). A model with a weak upper mantle viscosity (5×10^{19} Pa s, model 120p0510 in Fig. 5A), that may be more representative of the shallow upper mantle below the rift system of the West Antarctic Ice Sheet (WAIS), under-predicts uplift rates at most sites, only just capturing the observed rate (within the 1-sigma uncertainty) at sites 5 and 2.

It is worth noting that even if reasonable variations in the adopted 1-D Earth model parameters could resolve the over-prediction in the present-day uplift rates, it would not explain the occurrence of the apparently stable grounding lines around the Weddell Sea located on reverse bed slopes.

In conclusion, it is not possible to resolve the over-prediction of present-day uplift rates and capture the observed spatial signal with reasonable variations in the adopted 1-D Earth model parameters. While we have only investigated the sensitivity of uplift rates to the adopted Earth model using the W12 ice model, we note that other Antarctic GIA models (Ivins et al., 2013; Peltier et al., 2004) also fail to entirely capture the observed spatial signal in the present-day uplift rates, particularly the near-zero/negative rate at site 4 (Fig. 9). We therefore hypothesize that reasonable perturbations to the Earth models adopted in these studies would similarly fail to reproduce the observed pattern of uplift rates in the Weddell Sea region.

ICE-6G_C (Argus et al., 2014) is a notable exception to the Antarctic GIA models discussed above as it does show agreement with the near zero/negative uplift rate at site 4. However, there is no description within Argus et al., (2014) of the ice retreat/advance mechanism invoked such that present-day interior subsidence is obtained. To some extent this model has been tuned to fit geodetic datasets and, in the absence of other constraints on past ice sheet extent, it is possible to reproduce the observed signal through a large range of ice loading scenarios. As such, our approach, which is based on direct observation of Late Holocene ice sheet variations for this region (Siegert et al., 2013) represents an advance on previous work.

3.3. Sensitivity of the modelled present-day uplift rates to the LGM–early Holocene ice-loading history

The modelled present-day uplift rates are compared with the observed (elastic-corrected) present-day uplift rates at the seven sites for the three revised LGM–early Holocene ice-loading simulations (Section 2.2.2) in Fig. 5B. This sensitivity study was designed to investigate whether revising the LGM-early Holocene deglaciation history can resolve the over-prediction produced using the W12 model (Fig. 4)

From these results it is apparent that the modelled present-day uplift rates are relatively insensitive to the pre-10 kyr BP ice-loading history of the Weddell Sea (Fig. 5B). At site 3 there is only a minor difference (less than 0.2 mm/yr) in the predicted uplift rates compared with W12. Simulating a slower retreat (LGMA) or thicker LGM ice sheet (LGMC) has minimal impact on the modelled uplift rates at all sites, with a maximum difference of 0.8 mm/yr (Fig. 5B). The simulated faster retreat (LGMB) reduced the predicted uplift rates, by up to 1.6 mm/yr (site 5 and site 1), but does not fully resolve the over-prediction produced by W12. The near-zero/negative uplift rate at site 4 is not reproduced by this model, which still over-predicts (considering the 1-sigma uncertainty) the uplift rate by 4.2 mm/yr (Fig. 5B). Therefore, although changes in the LGM–early Holocene ice-loading history do impact on the modelled present-day uplift rates, they are not sufficient to resolve the over-prediction in W12 or capture the observed spatial variation. This weak sensitivity of the modelled uplift rate to the LGM–early Holocene deglaciation history was also found by Whitehouse et al., (2012b).

3.4. Sensitivity of the modelled present-day uplift rates to the spatial pattern of Holocene ice loading.

Using the three minimum ice extent scenarios (W12_Thin, W12_Min, W12_Max), we first investigate whether comparing modelled and observed uplift rates allows us to distinguish between the two hypotheses proposed by Siegert et al., (2103).

From Fig. 6 it is clear that the W12_Thin scenario does not reproduce the observed uplift rates, with only a minor reduction in the WRMSE from 3.31 mm/yr to 3.09 mm/yr compared with the W12 model. We therefore conclude that load changes associated with flow reorganization and thinning of the BIR are insufficient to explain the geodetic observations.

In contrast, the W12_Min and W12_Max scenarios tend to produce lower uplift rate predictions; the WRMSE for these scenarios is 1.55 mm/yr and 1.52 mm/yr, respectively. Although the W12_Max scenario has a lower WRMSE we note that this model results in a very large misfit at site 3 (1.6 mm/yr; see Fig. 6). This site is most sensitive to differences in the amount of retreat across the Robin subglacial basin (see Fig. 1A), and since the data at the other sites do not allow us to distinguish between the two models, we therefore adopt W12_Min as the most likely configuration of the ice sheet during its retreated phase. This W12_Min model is used to investigate the sensitivity of uplift rates to the timing of retreat (see Table 1 and Section 4).

4. Main Results and Discussion:

4.1. Results for the revised Late-Holocene ice-loading simulations

The WRMSE and mean bias for each of the 23 Late Holocene ice-loading simulations are summarized in Table 1. Figure 7 is a 3D representation of the WRMSE; results are plotted according to the initiation (kyr BP) of the extended retreat, the timing of the end of readvance and the duration of the stillstand (kyr) within each model.

In all of the 23 retreat-readvance ice-loading simulations (see supplementary material, Fig. 4 and Fig. 7) the over-prediction seen in the W12 model and the WRMSE are both significantly reduced, by at least 1 mm/yr in all cases.

The lowest WRMSE is produced in models where a stillstand is combined with a late readvance (ending at 0 kyr BP, e.g. W12_6i), as shown by the cluster of low WRMSE values (less than 1.6mm/yr) on the lowest level of the cube in Fig. 7. The WRMSE is higher in simulations with either no stillstand (W12_6, W12_5 and W12_4) or a short (1 kyr/no) stillstand combined with an early readvance (e.g. W12_6c, W12_5g), where the present-day extent is reached by 2 kyr BP (see Fig. 4).

The four models with the lowest WRMSE (less than 1.6 mm/yr; W12_6i, W12_6j, W12_6g and W12_6k) are characterized by an early retreat behind the grounding line defined in the W12 model (at 6 kyr BP), a relatively long stillstand, and a short readvance that continues to present day (Table 1 and Fig. 4). However, the duration of the retreat period is different between these four models, from 3 kyr in W12_6i to 1 kyr in W12_6k. This implies that the present-day uplift rate is less sensitive to the duration of retreat than to the timing of retreat; any decrease in the duration of retreat can be offset by a corresponding increase in the duration of the stillstand.

Specifically, with these four models the pronounced spatial variation, including the near zero/negative uplift at site 4, is reproduced. Only at site 1, where the misfit is reduced by up to 1.8 mm/yr, is the over-prediction not fully resolved, although this could plausibly be further reduced with additional refinement to our ice loading history (see Fig. 3), such as an increase in the spatial extent of the retreat-readvance of the grounded ice margin in this region.

As the Holocene deglacial history of the four revised models shown in Fig. 4 is relatively similar (See Table 1) the difference in the modelled present-day uplift rates is very small (less than the 1-sigma uncertainty). Consequently, this modelling approach does not allow us to determine a precise timing for the revised Late Holocene deglacial history. However, for the discussion that follows we use the W12_6i model as it has the lowest WRMSE; 1.55 mm/yr (see Fig. 7 and Table 1). Given the similarity in the deglaciation history of the four models shown in Fig. 4, the general results and conclusions relating to the W12_6i model are likely to also apply to the other three models.

4.2: Impact of the revised Holocene ice-loading simulation on bedrock elevation and grounding line location

Returning to the initial aim outlined in the Introduction, we explore the effect of the revised retreat scenario on bedrock elevation during the Late Holocene, and the consequent position of the grounding line.

Differences in the change in bedrock elevation between W12 and W12_6i are shown in Fig. 8 for a range of time intervals. Between 6 - 3 kyr BP (Fig. 8A) the bedrock uplifts by up to an additional 40 m for the W12_6i model compared with W12, driven by the reduction in the overlying load as the ice sheet retreats and thins. During the 1 kyr stillstand (Fig. 8B) the time-delayed viscous response to this recent retreat means that the bedrock continues to uplift faster in the W12_6i model, but during the short readvance (Fig. 8C) the increase in surface loading produces an associated fall in the bedrock height, generating subsidence at site 4 (see Fig. 4).

The pronounced change in bedrock elevation driven by this revised deglacial history would have resulted in a significant change in the position of the grounding line within the IIS, the MIS, and across the BIR, and this would have driven localized changes in ice dynamics, that could include a reorganization of the flow within the ice streams.

These results therefore support the second hypothesis proposed by Siegert et al., (2013); that of grounding line retreat inland of the present-day position, followed by a re-grounding driven by bedrock uplift, and subsequent readvance of the grounding line back towards the present-day location. The alternative hypothesis (simulated in W12_Thin), suggesting that glaciological data at BIR may be explained by internal reorganization of ice flow without retreat and readvance (Siegert et al., 2013), would not explain the GPS-observed region-wide pattern of deformation or explain the location of present-day grounding lines on reverse bed slopes; our revised model provides an explanation for both.

Further exploration of such late Holocene reorganization requires a coupled ice sheet-GIA model (Gomez et al., 2013) to fully account for the complex feedbacks that control grounding line migration. These include time-varying pertubations in local sea level (Gomez et al., 2012), accumulation, ice viscosity (Schoof, 2007), dynamism of bed friction (Sergienko and Hindmarsh, 2013) and changes in the stabilising effect of the surrounding ice shelves (Gudmundsson, 2013) through basal melting induced by ocean temperature changes (Pollard and DeConto, 2009; Hellmer et al., 2012). Whether the readvance proposed in our revised model is due to external forcing (e.g., less warm water penetrating under the FRIS) or internal dynamics (e.g., GIA uplift leading to bed shallowing and grounding line readvance) is difficult to resolve by ice-sheet modelling owing to the sensitivity of grounding-line motion to melt, but either process could have operated here or in other areas of the WAIS such as the Amundsen Sea embayment and the Ross Sea (Bindschadler et al., 1990; Catania et al., 2006). The possibility that some of these grounding lines might currently be advancing has implications for forecasting their response to warming associated with global change, as the initiation of unstable retreat would require changes in controls such as sub ice-shelf melt.

4.3: Comparison to alternative GIA models.

In Figure 9 the results from the W12 and W12_6i models are compared with the results from two other GIA models; IJ05_R2 (Ivins et al., 2013) and ICE-5G (Peltier, 2004), which have both been adopted in the correction of Gravity Recovery and Climate Experiment (GRACE) data (Velicogna and Wahr, 2006; Shepherd et al., 2012; Ivins et al., 2013). Regionally there is general agreement in the modelled uplift rates across the AIS between W12, W12_6i and IJ05_R2, with all of the models predicting subsidence across most of the interior of East Antarctica and uplift across the WAIS. In contrast, ICE-5G and ICE-6G_C (Argus et al., 2014) predict uplift across most of East Antarctica. There are, however, greater differences around the Weddell Sea where the maximum uplift rate is > 10 mm/yr in the W12 and ICE-5G models compared with 7 mm/yr and 2.5 mm/yr in the W12_6i and IJ05_R2 models, respectively. In particular, the W12_6i model predicts a subsidence of ~ -2 mm/yr to the west of the Ellsworth mountain range, induced by the simulated readvance of the ice sheet across this region. This trend is markedly different to the pattern of present-day uplift around the Weddell Sea predicted by the other three recent Antarctic GIA models (Fig. 9). Our revised Holocene ice-loading history might have important implications for the GIA correction applied to the GRACE data, likely resulting in a reduction in the GIA correction and a smaller estimate of present-day ice mass loss within the Weddell Sea region of the WAIS (King et al., 2012).

5. Concluding discussion

In this study we have addressed two outstanding unresolved issues in the Weddell Sea: (i) the widespread occurrence of ice streams on reverse bed slopes; and (ii) the inability of most current GIA models, which adopt a monotonic retreat pattern for the WAIS within the Weddell Sea, to match present-day bedrock uplift rates.

We have shown that by revising the Late Holocene deglaciation pattern within the Weddell Sea to include an early retreat behind the grounding line defined in the W12 model (at 6 kyr BP) and a relatively long stillstand followed by a short readvance that continues to present day, we can explain these two observations. With regard to the GPS-derived uplift rates (Thomas et al., 2011), such a model reproduces the spatial pattern and magnitude at almost all GPS sites, including the observation of near-zero/negative uplift within the ice sheet interior, with the WRMSE reduced from 3.31 mm/yr (unmodified W12) to 1.59 mm/yr. This revised Late Holocene ice-loading simulation implies that the volume change of the AIS during the Late Holocene may have been more complex than previously posited; testing such a hypothesis should be an important target for future modelling and data studies.

An important consideration is the uniqueness of the results. Our WRMSE metric indicates that there is not a great deal of difference between the W12_min and W12_max configurations, and it may be that the total retreat is poorly constrained by this metric. A secondary metric of improved match at Site 3 distinguishes these hypotheses, favouring W12_min. It is of course true that loadings with shorter wavelength variation than the model resolution will give equally good fits, but these are not constrained by data and are unlikely to be sustainable glaciological configurations.

A key implication suggested by our revised ice-loading simulation is that some current ice margins on reverse bed slopes around the West Antarctic Ice Sheet are unstable, in agreement with theory (Schoof, 2007), but are advancing. There are currently three hypotheses for the existence of grounding-lines on reverse bed slopes. Two are process-based, the mechanical 'buttressing' hypothesis (Gudmundsson, 2012) and the GIA stabilization hypothesis (Gomez et al., 2013), and the third is our unstable advance hypothesis, which is a consequence of history. At present, the first two are theoretical arguments based on good models of ice dynamics but without empirical evidence, while ours has empirical backing, but should be tested by process-based modelling, adding a proper ice-dynamics component to our solid earth modelling.

The possibility of ice sheets being in configurations promoting unstable advance has implications for forecasting the response of grounding lines to future warming, as the transition to unstable retreat would require a change in controls such as sub ice-shelf melt rates (Joughin et al., 2014; Rignot et al., 2014). Finally, the revised Holocene ice-loading history proposed in our study might have important implications for the GIA correction applied to the GRACE data, with a likely reduction in the GIA correction producing a smaller estimate of the present-day ice loss around the Weddell Sea than previously suggested (King et al., 2012).

References

Argus, D.F., Blewitt, G., Peltier, W.R., Kreemer, C., 2011. Rise of the Ellsworth mountains and parts of the East Antarctic coast observed with GPS. Geophys Res Lett 38.

Argus, D.F., Peltier, W.R., 2010. Constraining models of postglacial rebound using space geodesy: a detailed assessment of model ICE-5G (VM2) and its relatives. Geophys J Int 181, 697-723.

Argus, D.F., Peltier, W.R., Drummond, R., Moore, A.W., 2014. The Antarctica component of postglacial rebound model ICE-6G_C (VM5a) based on GPS positioning, exposure age dating of ice thicknesses, and relative sea level histories. Geophys J Int.

Bentley, M.J., Fogwill, C.J., Le Brocq, A.M., Hubbard, A.L., Sugden, D.E., Dunai, T.J., Freeman, S.P.H.T., 2010. Deglacial history of the West Antarctic Ice Sheet in the Weddell Sea embayment: Constraints on past ice volume change. Geology 38, 411-414.

Bevis, M., Kendrick, E., Smalley, R., Dalziel, I., Caccamise, D., Sasgen, I., Helsen, M., Taylor, F.W., Zhou, H., Brown, A., Raleigh, D., Willis, M., Wilson, T., Konfal, S., 2009. Geodetic measurements of vertical crustal velocity in West Antarctica and the implications for ice mass balance. Geochem Geophy Geosy 10.

Bindschadler, R., Roberts, E.P., Iken, A., 1990. Age of the Crary Ice Rise, Antarctica, Determined from Temperature-Depth Profiles. Annals of Glaciology 14, 13-16.

Catania, G.A., Conway, H., Raymond, C.F., Scambos, T.A., 2006. Evidence for floatation or near floatation in the mouth of Kamb Ice Stream, West Antarctica, prior to stagnation. J Geophys Res-Earth 111.

Chaput, J., Aster, R.C., Huerta, A., Sun, X., Lloyd, A., Wiens, D., Nyblade, A., Anandakrishnan, S., Winberry, J.P., Wilson, T., 2014. The crustal thickness of West Antarctica. Journal of Geophysical Research: Solid Earth 119.

Conway, H., Hall, B.L., Denton, G.H., Gades, A.M., Waddington, E.D., 1999. Past and future grounding-line retreat of the West Antarctic Ice Sheet. Science 286, 280-283.

Dziewonski, A.M., Anderson, D.L., 1981. Preliminary Reference Earth Model. Physics of the Earth and Planetary Interiors 25, 297-356.

Fretwell, P., Pritchard, H.D., Vaughan, D.G., Bamber, J.L., Barrand, N.E., Bell, R., Bianchi, C., Bingham, R.G., Blankenship, D.D., Casassa, G., Catania, G., Callens, D., Conway, H., Cook, A.J., Corr, H.F.J., Damaske, D., Damm, V., Ferraccioli, F., Forsberg, R., Fujita, S., Gim, Y., Gogineni, P., Griggs, J.A., Hindmarsh, R.C.A., Holmlund, P., Holt, J.W., Jacobel, R.W., Jenkins, A., Jokat, W., Jordan, T., King, E.C., Kohler, J., Krabill, W., Riger-Kusk, M., Langley, K.A., Leitchenkov, G., Leuschen, C., Luyendyk, B.P., Matsuoka, K., Mouginot, J., Nitsche, F.O., Nogi, Y., Nost, O.A., Popov, S.V., Rignot, E., xRippin, D.M., Rivera, A., Roberts, J., Ross, N., Siegert, M.J., Smith, A.M., Steinhage, D., Studinger, M., Sun, B., Tinto, B.K., Welch, B.C., Wilson, D., Young, D.A., Xiangbin, C., Zirizzotti, A., 2013. Bedmap2: improved ice bed, surface and thickness datasets for Antarctica. Cryosphere 7, 375-393.

Gomez, N., Pollard, D., Mitrovica, J.X., 2013. A 3-D coupled ice sheet – sea level model applied to Antarctica through the last 40 ky. Earth Planet Sc Lett 384, 88-99.

Gomez, N., Pollard, D., Mitrovica, J.X., Huybers, P., Clark, P.U., 2012. Evolution of a coupled marine ice sheet-sea level model. Journal of Geophysical Research: Earth Surface 117.

Gudmundsson, G.H., 2013. Ice-shelf buttressing and the stability of marine ice sheets. Cryosphere 7, 647-655.

Hellmer, H.H., Kauker, F., Timmermann, R., Determann, J., Rae, J., 2012. Twenty-first-century warming of a large Antarctic ice-shelf cavity by a redirected coastal current. Nature 485, 225-228.

Hemer, M.A., Harris, P.T., 2003. Sediment core from beneath the Amery Ice Shelf, East Antarctica, suggests mid-Holocene ice-shelf retreat. Geology 31, 127-130.

Hillenbrand, C.-D., Bentley, M.J., Stolldorf, T.D., Hein, A.S., Kuhn, G., Graham, A.G.C., Fogwill, C.J., Kristoffersen, Y., Smith, J.A., Anderson, J.B., Larter, R.D., Melles, M., Hodgson, D.A., Mulvaney, R., Sugden, D.E., 2013. Reconstruction of changes in the Weddell Sea sector of the Antarctic Ice Sheet since the Last Glacial Maximum. Quaternary Sci Rev.

Ivins, E.R., James, T.S., Wahr, J., O. Schrama, E.J., Landerer, F.W., Simon, K.M., 2013. Antarctic contribution to sea level rise observed by GRACE with improved GIA correction. Journal of Geophysical Research: Solid Earth 118, 3126-3141.

Ivins, E.R., Raymond, C.A., James, T.S., 2000. The influence of 5000 year-old and younger glacial mass variability on present-day crustal rebound in the Antarctic Peninsula. Earth Planets Space 52, 1023-1029.
Joughin, I., Alley, R.B., 2011. Stability of the West Antarctic ice sheet in a warming world. Nat Geosci 4, 506-513.
Joughin, I., Bamber, J.L., 2005. Thickening of the ice stream catchments feeding the Filchner-Ronne Ice Shelf, Antarctica. Geophys Res Lett 32.
Kendall, R.A., Mitrovica, J.X., Milne, G.A., 2005. On post-glacial sea level - II. Numerical formulation and comparative results on spherically symmetric models. Geophys J Int 161, 679-706.
King, M.A., Bingham, R.J., Moore, P., Whitehouse, P.L., Bentley, M.J., Milne, G.A., 2012. Lower satellite-gravimetry estimates of Antarctic sea-level contribution. Nature 491, 586-589.
Lambeck, K., Smither, C., Johnston, P., 1998. Sea-level change, glacial rebound and mantle viscosity for northern Europe. Geophys J Int 134, 102-144.
Lambrecht, A., Sandhager, H., Vaughan, D.G., Mayer, C., 2007. New ice thickness maps of Filchner-Ronne Ice Shelf, Antarctica, with specific focus on grounding lines and marine ice. Antarct Sci 19, 521-532.
Le Brocq, A.M., Bentley, M.J., Hubbard, A., Fogwill, C.J., Sugden, D.E., Whitehouse, P.L., 2011. Reconstructing the Last Glacial Maximum ice sheet in the Weddell Sea embayment, Antarctica, using numerical modelling constrained by field evidence. Quaternary Sci Rev 30, 2422-2432.
Milne, G.A., Mitrovica, J.X., 1998. Postglacial sea-level change on a rotating Earth. Geophys J Int 133, 1-19.
Milne, G.A., Mitrovica, J.X., Scherneck, H.G., Davis, J.L., Johansson, J.M., Koivula, H., Vermeer, M., 2004. Continuous GPS measurements of postglacial adjustment in Fennoscandia: 2. Modeling results. Journal of Geophysical Research: Solid Earth 109.
Mitrovica, J.X., Davis, J.L., Shapiro, I.I., 1994. A Spectral Formalism for Computing 3-Dimensional Deformations Due to Surface Loads .1. Theory. Journal of Geophysical Research: Solid Earth 99, 7057-7073.
Mitrovica, J.X., Forte, A.M., 2004. A new inference of mantle viscosity based upon joint inversion of convection and glacial isostatic adjustment data. Earth Planet Sc Lett 225, 177-189.
Mitrovica, J.X., Milne, G.A., Davis, J.L., 2001. Glacial isostatic adjustment on a rotating earth. Geophys J Int 147, 562-578.
Mitrovica, J.X., Wahr, J., Matsuyama, I., Paulson, A., 2005. The rotational stability of an ice-age earth. Geophys J Int 161, 491-506.
Morelli, A., Danesi, S., 2004. Seismological imaging of the Antarctic continental lithosphere: a review. Global and Planetary Change 42, 155-165.
Peltier, W.R., 2004. Global glacial isostasy and the surface of the ice-age earth: The ICE-5G (VM2) model and GRACE. Annual Review of Earth and Planetary Sciences 32, 111-149.
Pollard, D., DeConto, R.M., 2009. Modelling West Antarctic ice sheet growth and collapse through the past five million years. Nature 458, 329-U389.
Ross, N., Bingham, R.G., Corr, H.F.J., Ferraccioli, F., Jordan, T.A., Le Brocq, A., Rippin, D.M., Young, D., Blankenship, D.D., Siegert, M.J., 2012. Steep reverse bed slope at the grounding line of the Weddell Sea sector in West Antarctica. Nat Geosci 5, 393-396.
Rutt, I.C., Hagdorn, M., Hulton, N.R.J., Payne, A.J., 2009. The Glimmer community ice sheet model. J Geophys Res-Earth 114.
Schoof, C., 2007. Ice sheet grounding line dynamics: Steady states, stability, and hysteresis. Journal of Geophysical Research: Earth Surface 112.

Sergienko, O.V., Hindmarsh, R.C.A., 2013. Regular Patterns in Frictional Resistance of Ice-Stream Beds Seen by Surface Data Inversion. Science 342, 1086-1089.
Shepherd, A., Ivins, E.R., Geruo, A., Barletta, V.R., Bentley, M.J., Bettadpur, S., Briggs, K.H., Bromwich, D.H., Forsberg, R., Galin, N., Horwath, M., Jacobs, S., Joughin, I., King, M.A., Lenaerts, J.T.M., Li, J.L., Ligtenberg, S.R.M., Luckman, A., Luthcke, S.B., McMillan, M., Meister, R., Milne, G., Mouginot, J., Muir, A., Nicolas, J.P., Paden, J., Payne, A.J., Pritchard, H., Rignot, E., Rott, H., Sorensen, L.S., Scambos, T.A., Scheuchl, B., Schrama, E.J.O., Smith, B., Sundal, A.V., van Angelen, J.H., van de Berg, W.J., van den Broeke, M.R., Vaughan, D.G., Velicogna, I., Wahr, J., Whitehouse, P.L., Wingham, D.J., Yi, D.H., Young, D., Zwally, H.J., 2012. A Reconciled Estimate of Ice-Sheet Mass Balance. Science 338, 1183-1189.
Siegert, M., Ross, N., Corr, H., Kingslake, J., Hindmarsh, R., 2013. Late Holocene ice-flow reconfiguration in the Weddell Sea sector of West Antarctica. Quaternary Sci Rev 78, 98-107.
Steffen, H., Kaufmann, G., 2005. Glacial isostatic adjustment of Scandinavia and northwestern Europe and the radial viscosity structure of the Earth's mantle. Geophys J Int 163, 801-812.
Thomas, I.D., King, M.A., Bentley, M.J., Whitehouse, P.L., Penna, N.T., Williams, S.D.P., Riva, R.E.M., Lavallee, D.A., Clarke, P.J., King, E.C., Hindmarsh, R.C.A., Koivula, H., 2011. Widespread low rates of Antarctic glacial isostatic adjustment revealed by GPS observations. Geophys Res Lett 38.
Velicogna, I., Wahr, J., 2006. Measurements of Time-Variable Gravity Show Mass Loss in Antarctica. Science 311, 1754-1756.
Whitehouse, P.L., Bentley, M.J., Le Brocq, A.M., 2012a. A deglacial model for Antarctica: geological constraints and glaciological modelling as a basis for a new model of Antarctic glacial isostatic adjustment. Quaternary Sci Rev 32, 1-24.
Whitehouse, P.L., Bentley, M.J., Milne, G.A., King, M.A., Thomas, I.D., 2012b. A new glacial isostatic adjustment model for Antarctica: calibrated and tested using observations of relative sea-level change and present-day uplift rates. Geophys J Int 190, 1464-1482.

Supplementary Materials

Supplementary Text: Section S1, S2 and S3.
Table S1 and S2.

Figures S1 and S6.

Acknowledgements:
This is a Past4future contribution no. 60. The research leading to these results has received funding from the European Union's Seventh Framework Programme (FP7/2007-2013) under grant agreement no. 243908, "PAST4FUTURE. Climate change - learning from the past climate", and from the UK NERC awards: NE/F014260/1, NE/F01466X/1, NE/J088176/1 and NE/J008087/1. M.A.K. is a recipient of an Australian Research Council Future Fellowship (project number FT110100207). P.L.W. is a recipient of a NERC Independent Research Fellowship (grant ref: NE/K009958/1). S.B, R.H and P.L.W designed the modelling study and SB carried out the modelling. All authors contributed to the writing of the paper. We thank E. Ivins for providing the IJ05_R2 predicted present-day uplift rates.

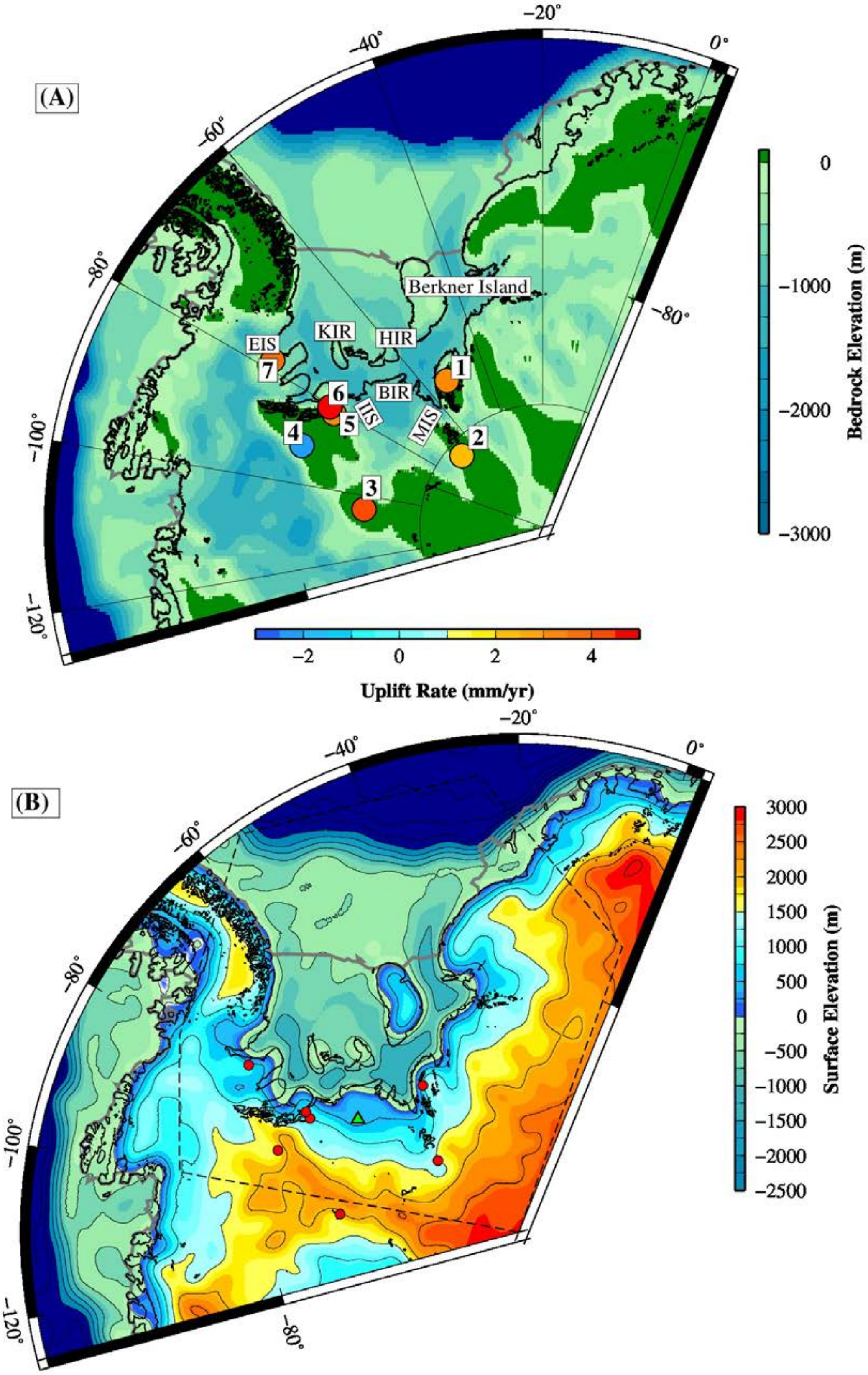
(A)
−20°
−40°
0°
−60°
−80°
−100°
−120°
−80°
Berkner Island
KIR
HIR
EIS
BIR
IIS
MIS
1
2
3
4
5
6
7
0
−1000
−2000
−3000
Bedrock Elevation (m)
−2
0
2
4
Uplift Rate (mm/yr)
(B)
−20°
−40°
0°
−60°
−80°
−100°
−120°
−80°
3000
2500
2000
1500
1000
500
0
−500
−1000
−1500
−2000
−2500
Surface Elevation (m)

Fig.1: Bedrock and ice sheet configuration of the Weddell Sea region. (A) Location map showing the seven GPS sites and their elastic-corrected present-day uplift rates, overlain on a map of the present-day bedrock topography (Fretwell et al., 2013) (see Table S1 for more site details). The black contour marks the present-day grounding line (see Bedmap2 (Fretwell et al., 2013)) and the solid grey line marks the present-day calving front. Labelled are the Bungenstock (BIR), Korff (KIR), and Henry (HIR) Ice Rises and the Institute (IIS), Möller (MIS) and Evans (EIS) Ice streams, with GPS site 7 located on the Fowler Peninsula. Areas of the bed above sea level are denoted by dark green shading; the Ellsworth Mountains lie approximately due north of GPS sites 5 and 6. (B) Present-day surface elevation of grounded ice, calculated by combining the present day ice thickness taken from the W12 ice model (Whitehouse et al., 2012a) with the present-day bedrock topography shown in (A). The grounding line position is only coarsely resolved in this model; this is sufficient for the purposes of GIA modelling. Bathymetry is shown in ice shelf regions and the open ocean. Red circles indicate GPS sites; the green triangle represents the location of the Robin Subglacial Basin.

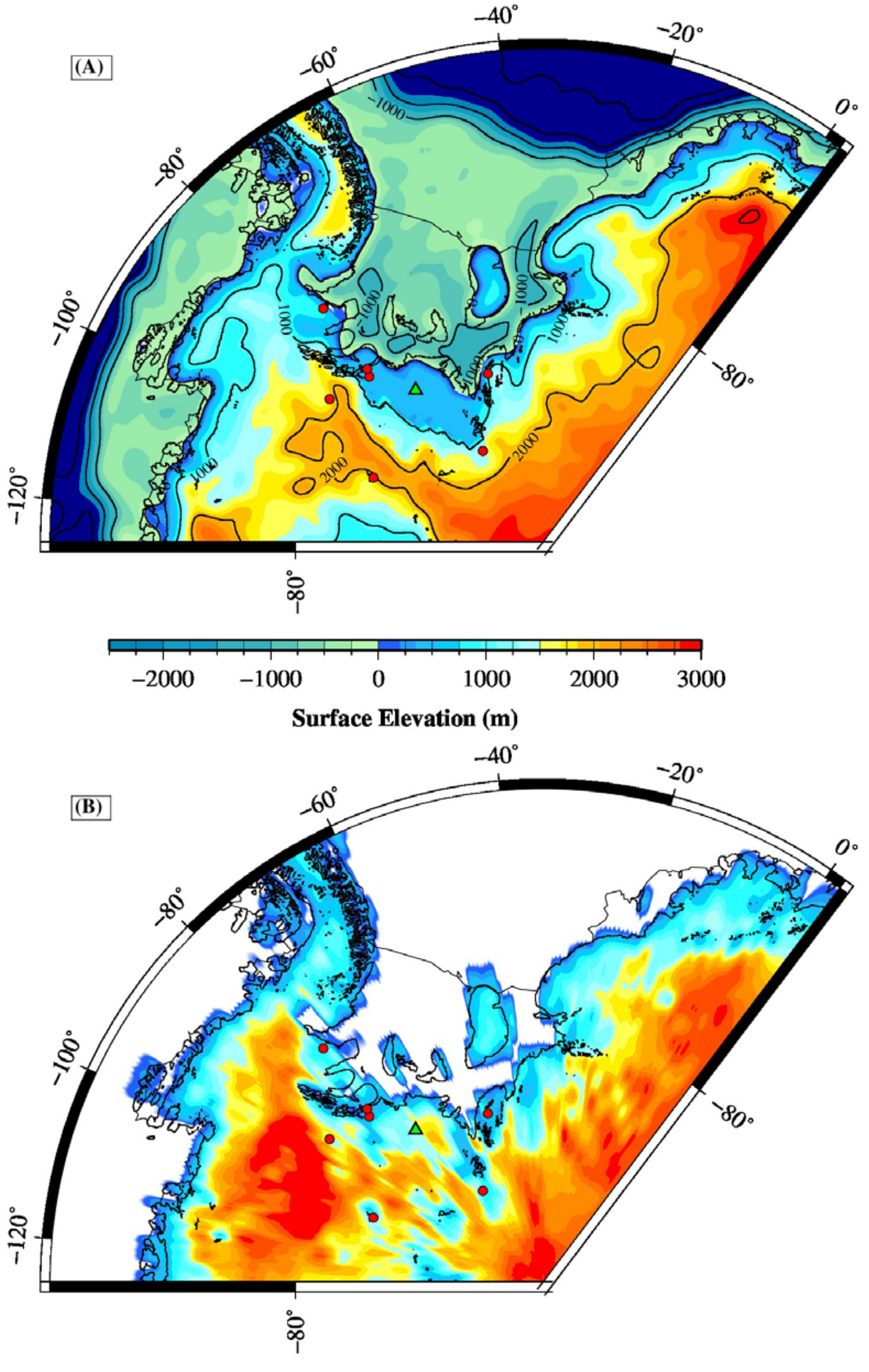

Fig.2. Surface elevation (A) and ice thickness (B) of the W12_Thin ice-loading simulation at the maximum thinned configuration. Red circles indicate GPS sites. Contours are drawn at 1000 m intervals. The green triangle represents the location of the Robin Subglacial Basin.

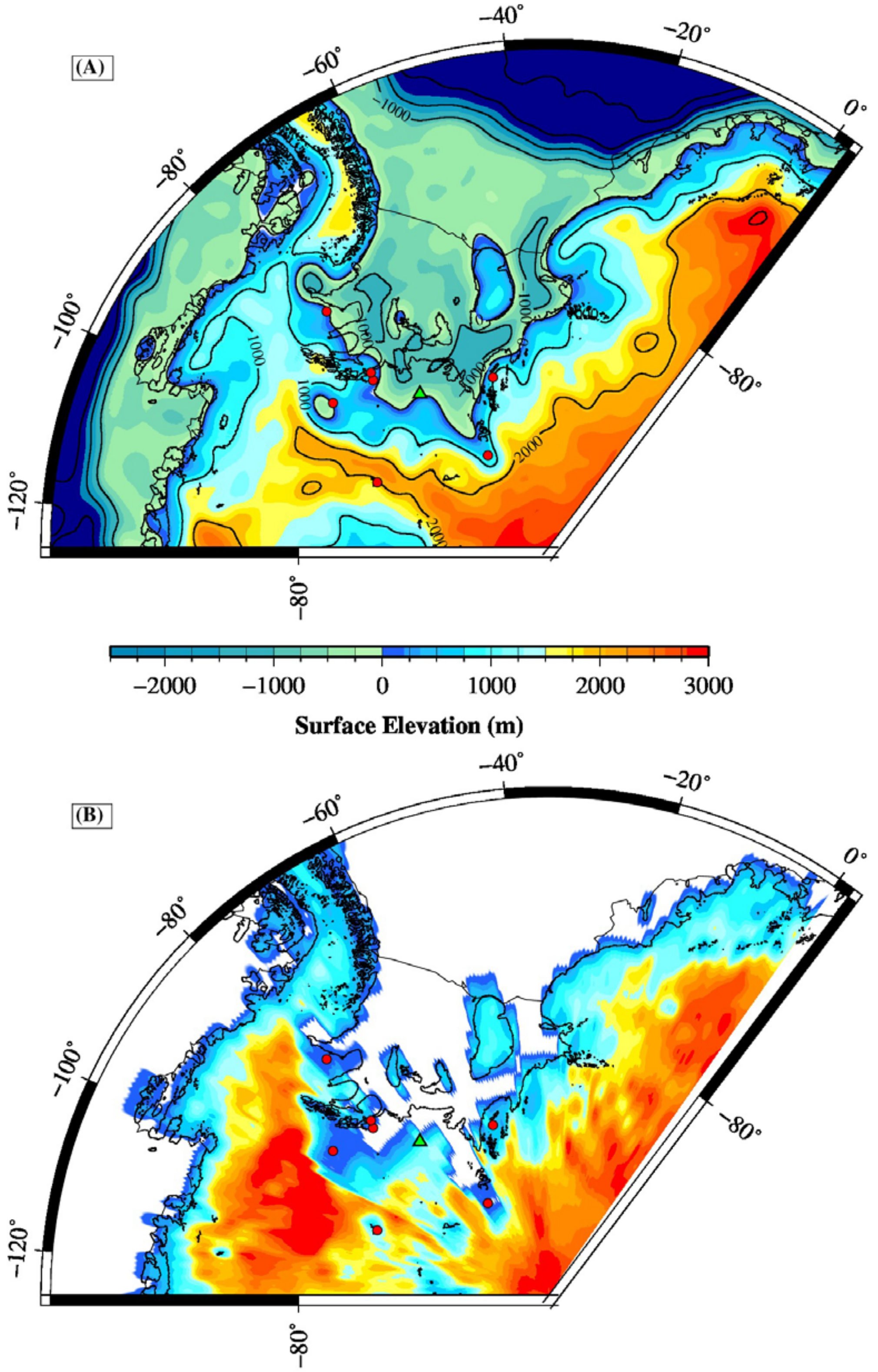
(A)
−40°
−20°
−60°
0°
−80°
−100°
−120°
−80°
−80°
−1000
1000
2000
−2000
−1000
0
1000
2000
3000
Surface Elevation (m)
(B)
−40°
−20°
−60°
0°
−80°
−100°
−120°
−80°
−80°

Fig.3. Surface elevation (A) and ice thickness (B) of the W12_Min ice-loading simulation at the maximum retreated extent. Red circles indicate GPS sites. The green triangle represents the location of the Robin Subglacial Basin. Contours are drawn at 1000m intervals.

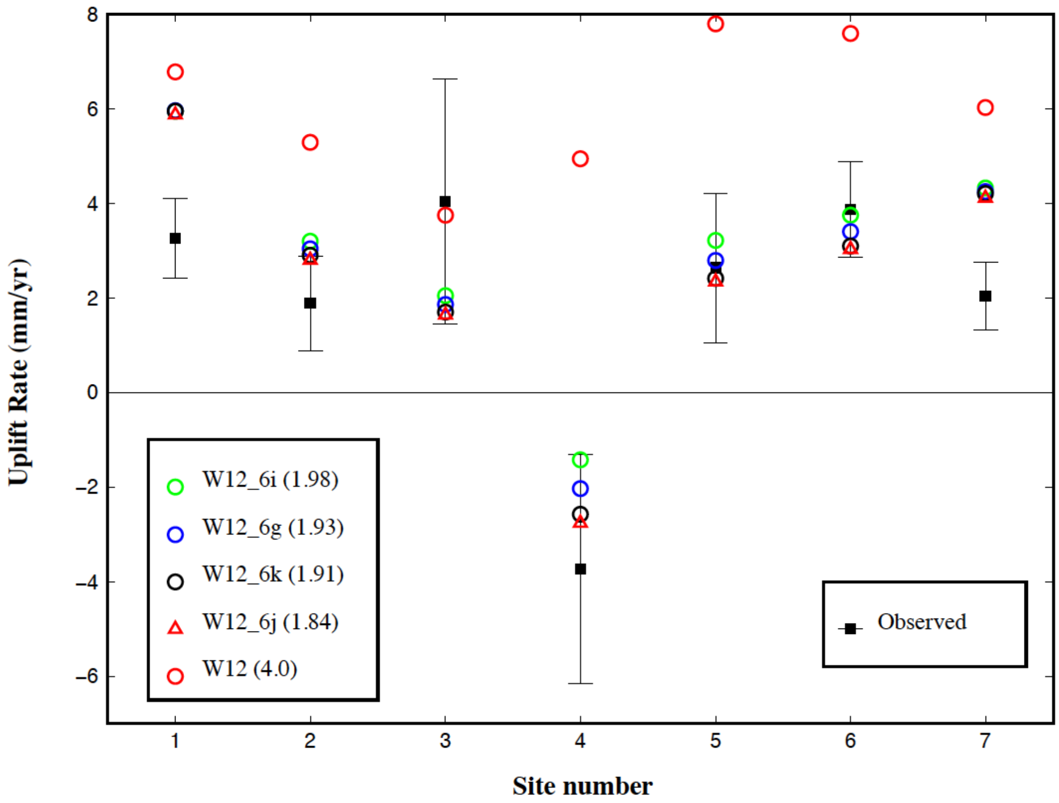

Fig.4. Observed (elastic-corrected) (black squares, with 1-sigma uncertainty) and modelled present-day uplift rate at the seven GPS sites, for W12 and the four revised ice-loading simulations with the lowest WRMSE (given in brackets, mm/yr). See Table 1 and main text for detailed information on these four revised simulations. Note the significant over-prediction of the W12 model, especially at site 4.

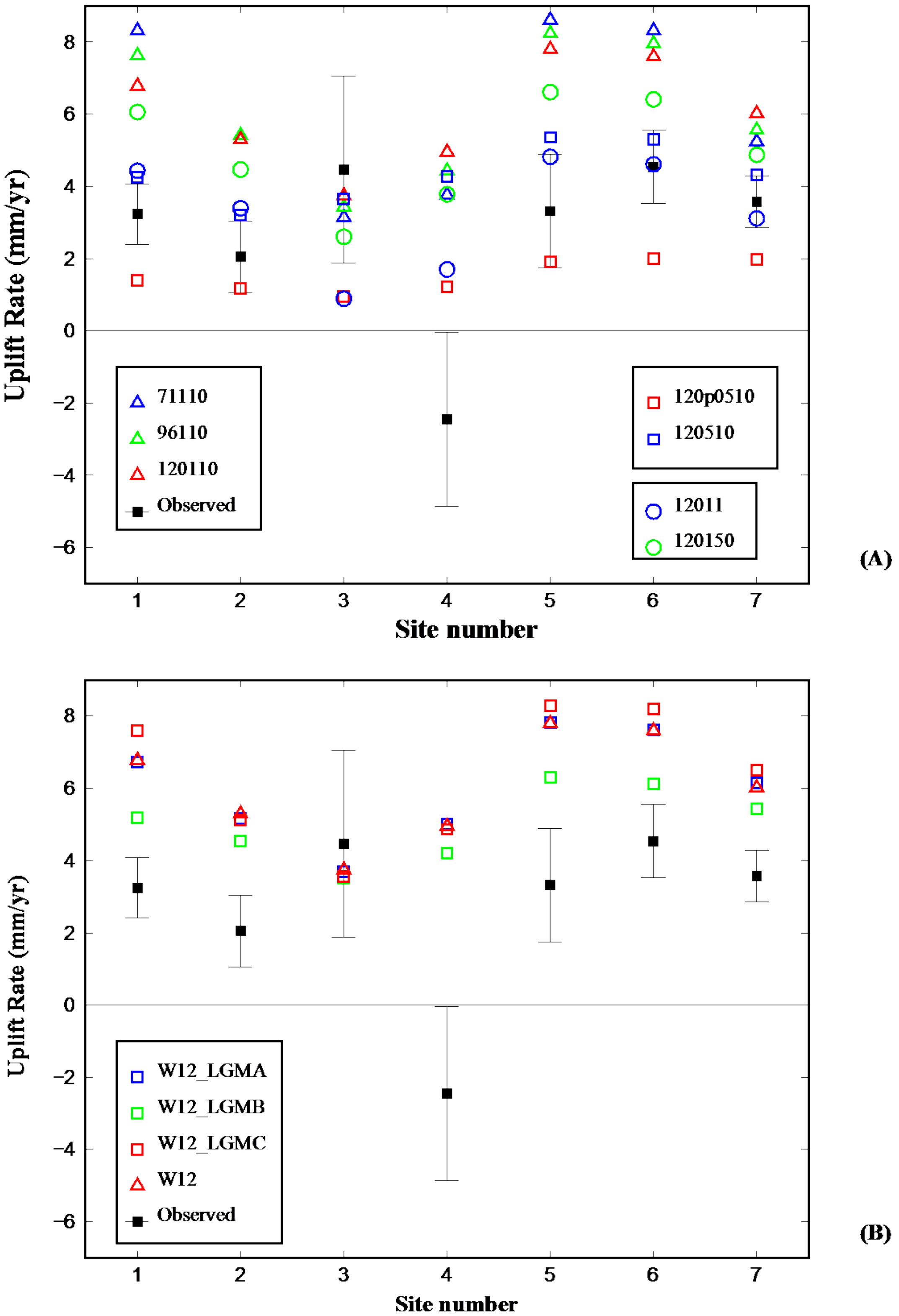

Fig. 5. (A) Observed (elastic-corrected) (black squares, with 1-sigma uncertainty) and modelled present-day uplift rates at the seven GPS sites for the seven Earth models listed in Table S2, using the W12 model. (B) Observed (elastic-corrected) (black squares, with 1-sigma uncertainty) and modelled present-day uplift rates at the seven GPS sites for the three

revised LGM–early Holocene ice-loading simulations as described in Section 2.2.2. The Earth model adopted has a lithospheric thickness of 120 km and upper and lower mantle viscosities of 1×10^{21} Pa s and 1×10^{22} Pa s, respectively.

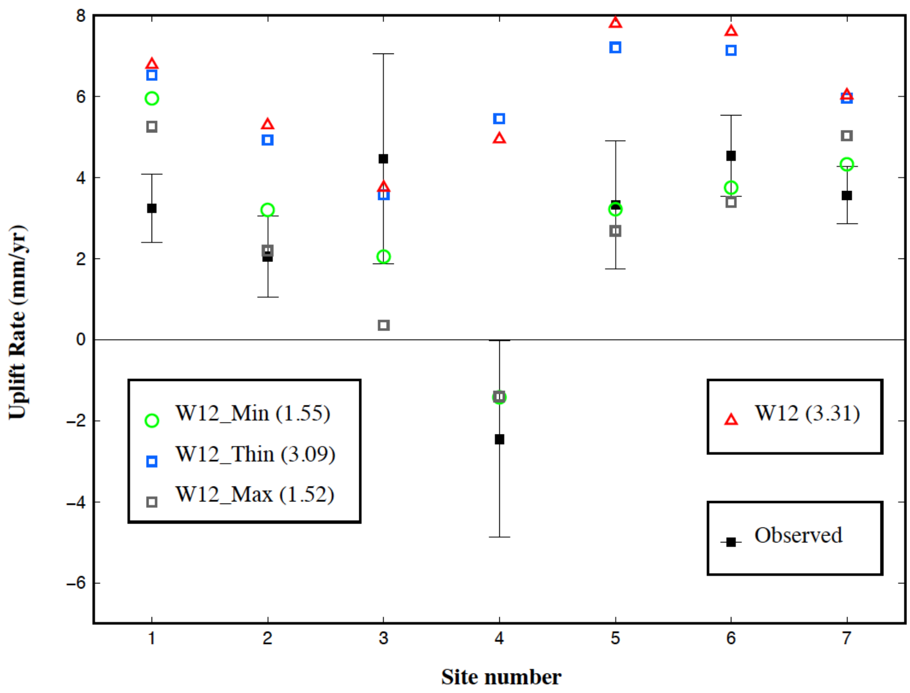

Fig. 6. Observed (elastic-corrected) (black squares, with1-sigma uncertainty) and modelled present-day uplift rates at the seven GPS sites for the W12, W12_Min, W12_Thin and W12_Max simulations, using an Earth model which has a lithospheric thickness of 120 km and upper and lower mantle viscosities of 1×10^{21} Pa s and 1×10^{22} Pa s, respectively. The estimated WRMSE (mm/yr) for each simulation is given in brackets.

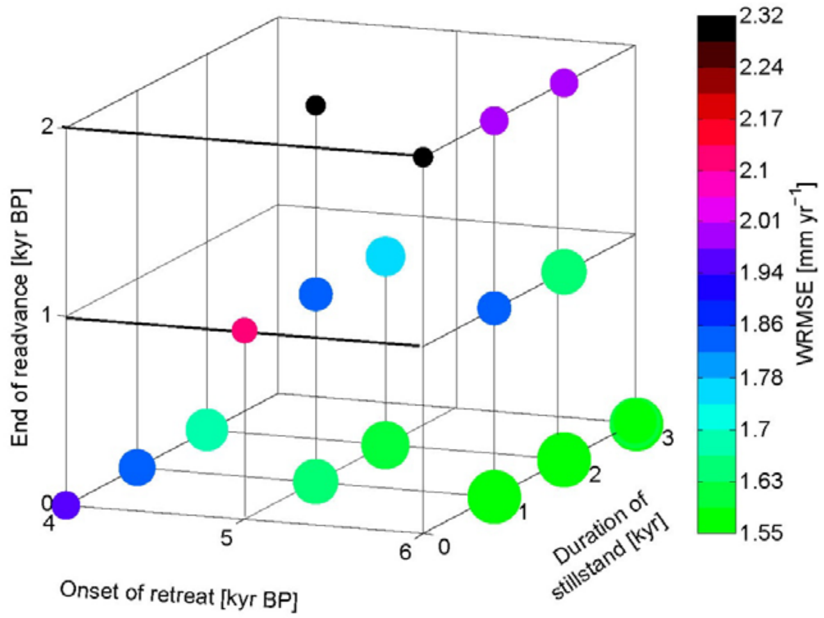

Fig.7. 3D spatial representation of the weighted-root mean square error (WRMSE) between the observed (elastic-corrected) and modelled uplift rates at each GPS site for the 23 ice model simulations listed in Table 1, comparing the initiation of the extended retreat (kyr BP), the timing of the end of readvance (kyr BP), and the duration of the stillstand (kyr). Note that the size of the circles is inversely proportional to the size of the WRMSE. The lowest WRMSE values are found in models with an early onset retreat (6 kyr BP), a late end of readvance (0 kyr BP) and a longer stillstand, which plot along the lower right hand edge of the cube. Note that it is not possible to explore the full parameter space of the cube given the time increments of the 23 models (see Table 1).

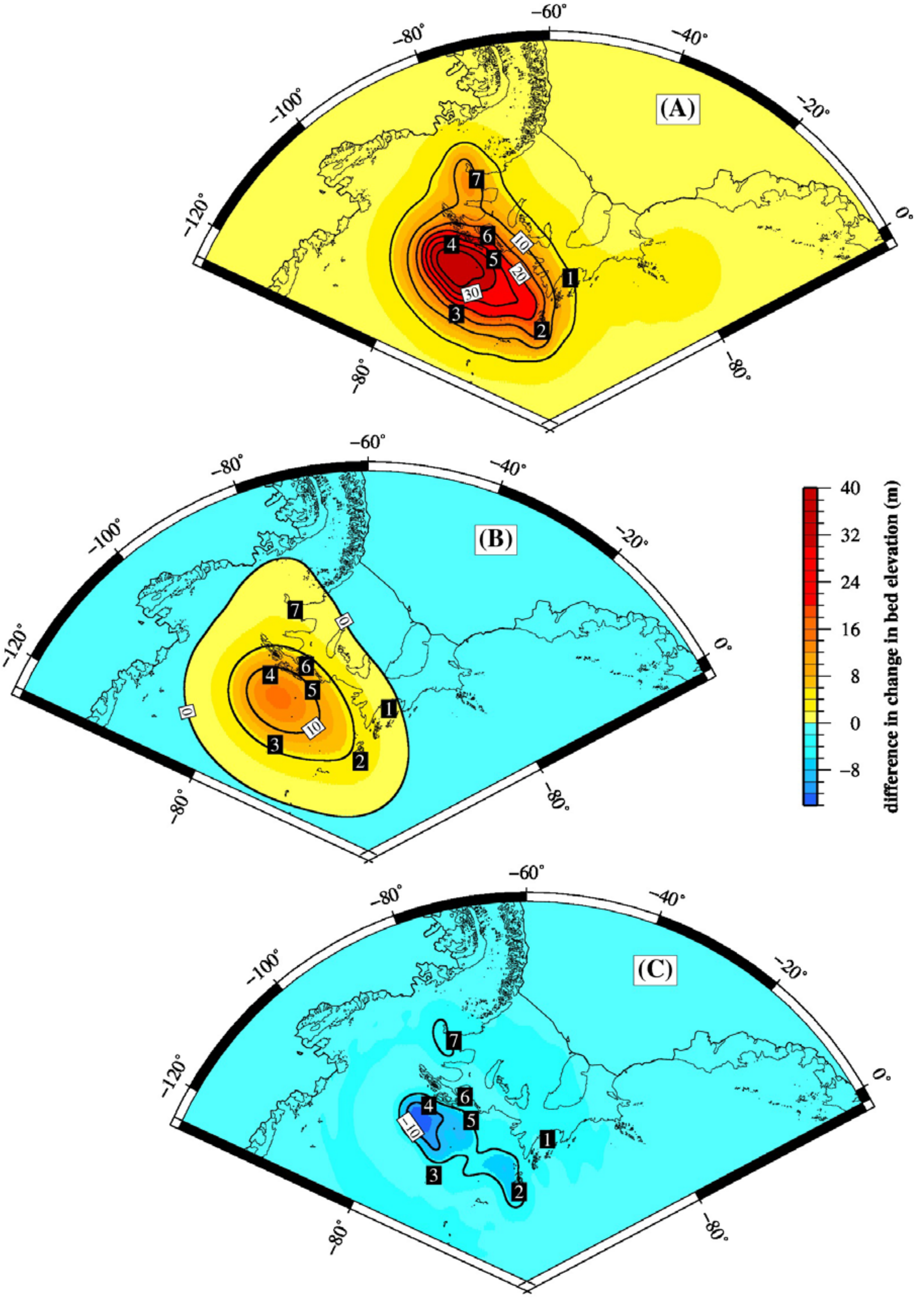
(A)
(B)
(C)
−60°
−80°
−40°
−100°
−20°
−120°
0°
−80°
−80°
1
2
3
4
5
6
7
10
20
30
0
10
−10
40
32
24
16
8
0
−8
difference in change in bed elevation (m)

Fig.8. Maps of the difference in the predicted change in bedrock elevation between the W12_6i and W12 models (W12_6i minus W12) over a range of time intervals: (A) 6-3 kyr BP (B) 3-2 kyr BP and (C) 2-0 kyr BP. Note that negative values indicate a relative fall in the bedrock height and positive values indicate a relative rise in the bedrock height over the specified time intervals compared with the W12 model. Black contours are drawn at 5 m intervals. The numbers mark the location of the 7 GPS sites, shown on Fig. 1A.

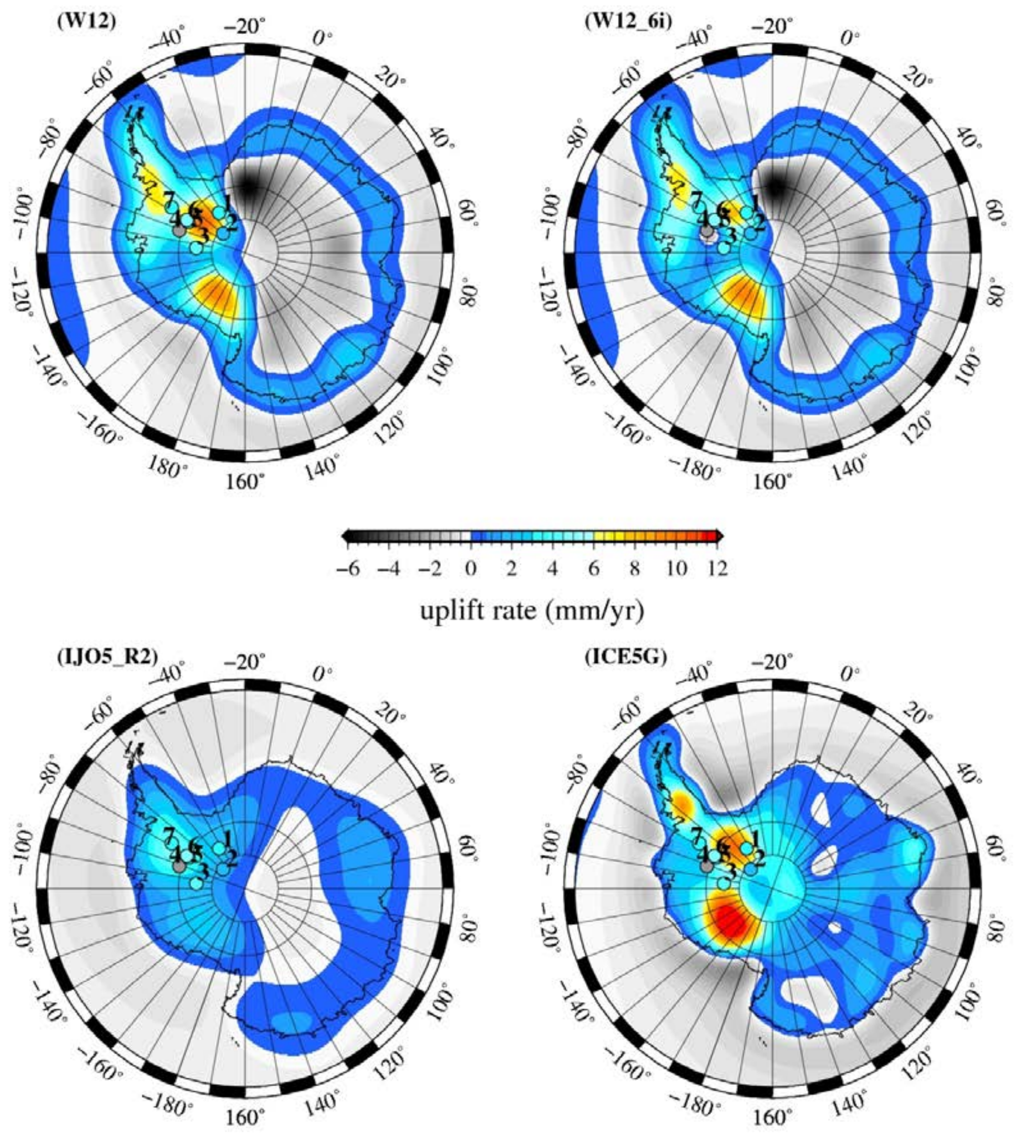

Fig. 9. Maps of the modelled present-day uplift rate for the W12 (Whitehouse et al., 2012a), W12_6i,(this study), IJ05_R2 (Ivins et al., 2013) and ICE-5G (Peltier, 2004) models. W12 and W12_6i predictions are generated using the optimum Earth model of Whitehouse et al.

(2012b), which has a lithospheric thickness of 120 km and upper and lower mantle viscosities of 1×10^{21} Pa s and 1×10^{22} Pa s, respectively, IJ05_R2 uses an Earth model with a lithospheric thickness of 65 km and upper and lower mantle viscosities of 2×10^{20} Pa s and 1.5×10^{21} Pa s, respectively, and ICE-5G uses VM2 with a 90 km lithospheric thickness (Peltier, 2004). The observed (elastic-corrected) uplift rates (see Table S1) at each GPS site are plotted using the same colour scheme as the predictions.

Table 1: The 26 ice-loading simulations used in this study and the calculated weighted root mean square error (WRMSE, mm/yr) and mean bias (mm/yr) for each simulation. In each simulation, apart from W12, W12_Thin and W12_Max, the W12_Min configuration is adopted for the maximum-retreated ice extent. Due to the timing of retreat adopted in W12_Min we note that this model is equivalent to W12_6i. The observed elastic-corrected (using the ICESat-derived loading model) uplift rates from Table S1 are used to calculate the WRMSE and mean bias. For each model simulation the timing (kyr BP) of the retreat, stillstand and readvance are given, with the duration (kyr) of each event given in brackets. A '0' in the stillstand column refers to models with no stillstand. Note that model names are defined in relation to the onset of the retreat; W12_6*- 6 kyr BP; W12_5*- 5 kyr BP, W12_4* - 4 kyr BP.

				Timing (kyr BP)		
Model Name		**WRMS(mm/yr)**	**Mean bias (mm/yr)**	**Retreat**	**Stillstand**	**Readvance**
W12_Max		1.52	-0.17	6--3(3)	3--2(1)	2--0(2)
W12_6i		1.55	0.33	6--3(3)	3--2(1)	2--0(2)
W12_6j		1.56	-0.24	6--4(2)	4--1(3)	1--0(1)
W12_6g		1.56	0.08	6--4(2)	4--2(2)	2--0(2)
W12_6k		1.59	-0.15	6--5(1)	5--2(3)	2--0(2)
W12_5d		1.62	0.41	5--4(1)	4--2(2)	2--0(2)
W12_6f		1.65	0.51	6--4(2)	4--2(2)	2--1(1)
W12_5e		1.66	0.68	5--3(2)	3--2(1)	2--0(2)
W12_4a		1.69	0.74	4--3(1)	3--1(2)	1--0(1)
W12_5c		1.77	0.83	5--4(1)	4--2(2)	2--1(1)
W12_6m		1.82	0.48	6--5(1)	5--3(2)	3--0(3)
W12_4b		1.82	1.06	4--3(1)	3--2(1)	2--0(2)
W12_6e		1.83	1.00	6--4(2)	4--3(1)	3--1(2)
W12_6h		1.84	0.71	6--4(2)	4--3(1)	3--0(3)
W12_5a		1.85	1.10	5--3(2)	3--2(1)	2--1(1)
W12_6d		1.89	0.30	6--5(1)	5--3(2)	3--1(2)
W12_4		1.96	1.40	4--2(2)	0	2--0(2)
W12_6l		2.01	1.33	6--5(1)	5--3(2)	3--2(1)
W12_6b		2.01	1.33	6--5(1)	5--4(1)	3--2(1)
W12_6a		2.10	1.56	6--4(2)	4--3(1)	3--2(1)
W12_5		2.11	1.60	5--3(2)	0	3--1(2)
W12_6c		2.21	1.71	6--5(1)	5--4(1)	4--2(2)
W12_5h		2.31	1.89	5--4(1)	4--3(1)	3--2(1)
W12_6		2.32	1.94	6--4(2)	0	4--2(2)
W12_Thin		3.09	3.15	6--3(3)	3--2(1)	2--0(2)

W12		3.31	3.35				

Supplementary Materials.

Section S1: GPS site information and Earth models

The details of the GPS sites and the range of Earth models used in the simulations are shown in Table S1 and S2, respectively.

Section S2: Surface elevation adopted during simulations.

Figures S1-S4 show the surface elevation configurations during the deglacial simulations.

Section S3: Comparing the modelled and observed present-day uplift rates at each GPS site for the 23 revised Late Holocene ice-loading simulations

The modelled and observed (elastic-corrected) present-day uplift rates at each GPS site are compared for a range of simulations to investigate the impact of changing the duration (kyr) and initiation (kyr BP) of the extended retreat and readvance (Fig.S5) and the duration (kyr) and timing (kyr BP) of the stillstand (Fig. S6). For more information on the timing and duration of the retreat-stillstand-readvance in each simulation, see Table.1.

Figure S5A compares the modelled uplift rates for simulations with the same ice-loading history from 3 kyr BP to present (a 1 kyr stillstand followed by a 2 kyr readvance, continuing to present day) but with a variable duration and initiation of the extended retreat. The difference in the modelled uplift rate between each simulation varies between sites; from less than 0.5 mm/yr at sites 1, 2, 3 and 7 up to between 1.0 and 1.4 mm/yr at sites 4, 5 and 6. This is to be expected as the latter three sites are closer to the area of maximum change in ice sheet extent and thickness (see Fig. 3). Despite this, the reduction in the over-prediction (i.e. at site 4) is greatest in the simulation with an earlier onset (6 kyr BP) and longer duration (3 kyr) retreat (W12_6i).

Figure S5B compares the modelled uplift rates for simulations, which have the same timing of retreat-stillstand, but varying duration (kyr) and timing (kyr BP) of readvance. Note that W12_6l, W12_6d and W12_6m have the same deglaciation history prior to 3 kyr BP (a retreat between 6-5 kyr BP followed by a 2 kyr stillstand) and W12_6f and W12_6g have the same deglaciation history prior to 2 kyr BP (a retreat between 6-4 kyr BP, followed by a 2 kyr stillstand) (See Table 1). Simulations where the readvance ends later (0 kyr BP, i.e. continuing to present-day) and is longer (W12_6g and W12_6m) produce a better fit to the observed (elastic-corrected) uplift rates. However, the predictions display a greater dependence on the timing of the end of the readvance than its duration. For example, a 1 kyr readvance is simulated in both W12_6l and W12_6f, yet the WRMSE is lower (2.0 mm/yr compared with 1.7 mm/yr), and the over-prediction is reduced (i.e. at site 4 (by 1.8 mm/yr), site 5 (by 1.2 mm/yr) and site 6 (by 1 mm/yr)) in the W12_6f model, where the readvance ends later (1 kyr BP compared with 2 kyr BP). This implies that the present-day uplift rate is less sensitive to the initiation and duration of the readvance than the time at which it ends.

From the modelled uplift rates in Fig. S6 it is apparent that the maximum reduction in the over-prediction is achieved in the simulations with a longer stillstand (3 kyr, W12_6j and W12_6k). However, there is a further dependence on the corresponding timing of the extended retreat and readvance. Figure S6A compares simulations with a short (1 kyr) but varying timing for the initiation of the extended retreat combined with the same readvance (2-0 kyr BP). An improved fit to the data is achieved with a short early (6 kyr BP) retreat and a long (3 kyr) stillstand (W12_6k) as opposed to a short late (4 kyr BP) retreat and short (1 kyr) stillstand (W12_4b). This follows from the results shown in Fig. S5A where the over-prediction is reduced in simulations with an early initiation (6 kyr BP) for the extended retreat. Comparing simulations with the same duration and timing of the extended retreat (between 6-4 kyr BP) (see Fig. S6B) an improved fit is achieved where both the stillstand and readvance end later (as shown in Fig. S5B).

Site No.	Site	Longitude	Latitude	Observed GPS Rate (mm/yr)	Sigma (mm/yr)	ICESat elastic Rate (mm/yr)	Mass flux elastic Rate (mm/yr)	ICESat-Adjusted Rate (mm/yr)	Mass flux-Adjusted Rate (mm/yr)
1	W04_AV	-53.20	-82.86	3.42	0.84	0.18	0.16	3.24	3.26
2	W02_AV	-68.55	-85.61	2.17	1.00	0.12	0.28	2.05	1.89
3	W09	-104.39	-82.68	4.54	2.59	0.07	0.49	4.47	4.05
4	W06A	-91.28	-79.63	-2.20	2.42	0.25	1.53	-2.45	-3.73
5	W07_AV	-81.43	-80.32	3.61	1.58	0.29	0.97	3.32	2.64
6	W05_AV	-80.56	-80.04	4.86	1.01	0.32	0.99	4.54	3.87
7	HAAG	-78.29	-77.04	3.47	0.71	-0.10	1.43	3.57	2.04

Table S1. Site information for the seven GPS sites used in the study, including the observed uplift rate, 1-sigma uncertainty and two modelled elastic rates, all of which are duplicated from supplementary material of Thomas et al., (2011) where full details may be found. Of the two elastic models of Thomas et al., (2011) we adopt the ICESat-derived model based on the work of Riva et al., (2009), as shown highlighted by shaded grey columns. The 'mass flux elastic rates' were estimated by Thomas et al. (2011) from an ice mass flux dataset (Rignot et al., 2008) with assumptions on the spatial pattern of mass loss; these are shown to provide a conservative measure of uncertainty in the elastic correction. The site numbers are used to indicate the location of the GPS receivers on Fig.1A. Where Thomas et al., (2011) list GPS uplift estimates for pairs of closely-located monuments (sites 1, 2, 5 and 6) we adopt the weighted-average rate for each site.

Name	Lithospheric Thickness (km)	Upper Mantle Viscosity (Pa s)	Lower Mantle Viscosity (Pa s)
71110	71 km	1×10^{21}	1×10^{22}
96110	96 km	1×10^{21}	1×10^{22}
120p0510	120 km	5×10^{19}	1×10^{22}

120110	120 km	1×10^{21}	1×10^{22}
120510	120 km	5×10^{21}	1×10^{22}
12011	120 km	1×10^{21}	1×10^{20}
120150	120 km	1×10^{21}	5×10^{22}

Table S2. The seven Earth models investigated. Results using these Earth models are shown in Fig. 3.

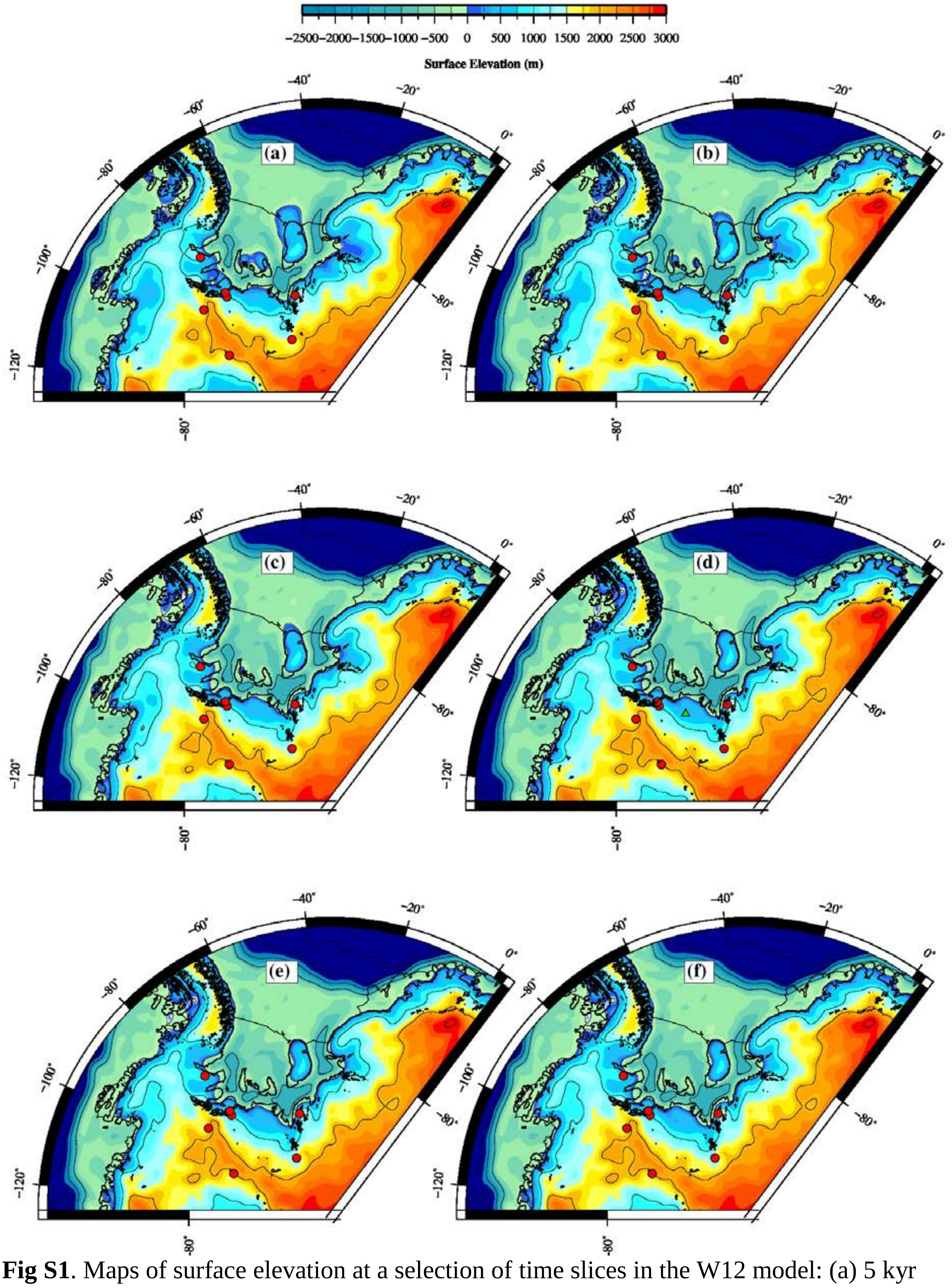

Fig S1. Maps of surface elevation at a selection of time slices in the W12 model: (a) 5 kyr BP, (b) 4 kyr BP, (c) 3 kyr BP, (d) 2 kyr BP, (e) 1 kyr BP and (f) 0 Kyr BP. This model assumes very little ice-sheet change during this period. GPS sites are indicated by red circles. The green triangle in plot (d) marks the location of the Robin Subglacial Basin. Contours are drawn at 1000 m intervals. Note that surface elevations greater than 3000 m are shown in red and bathymetry below -2500 m is shown in dark blue.

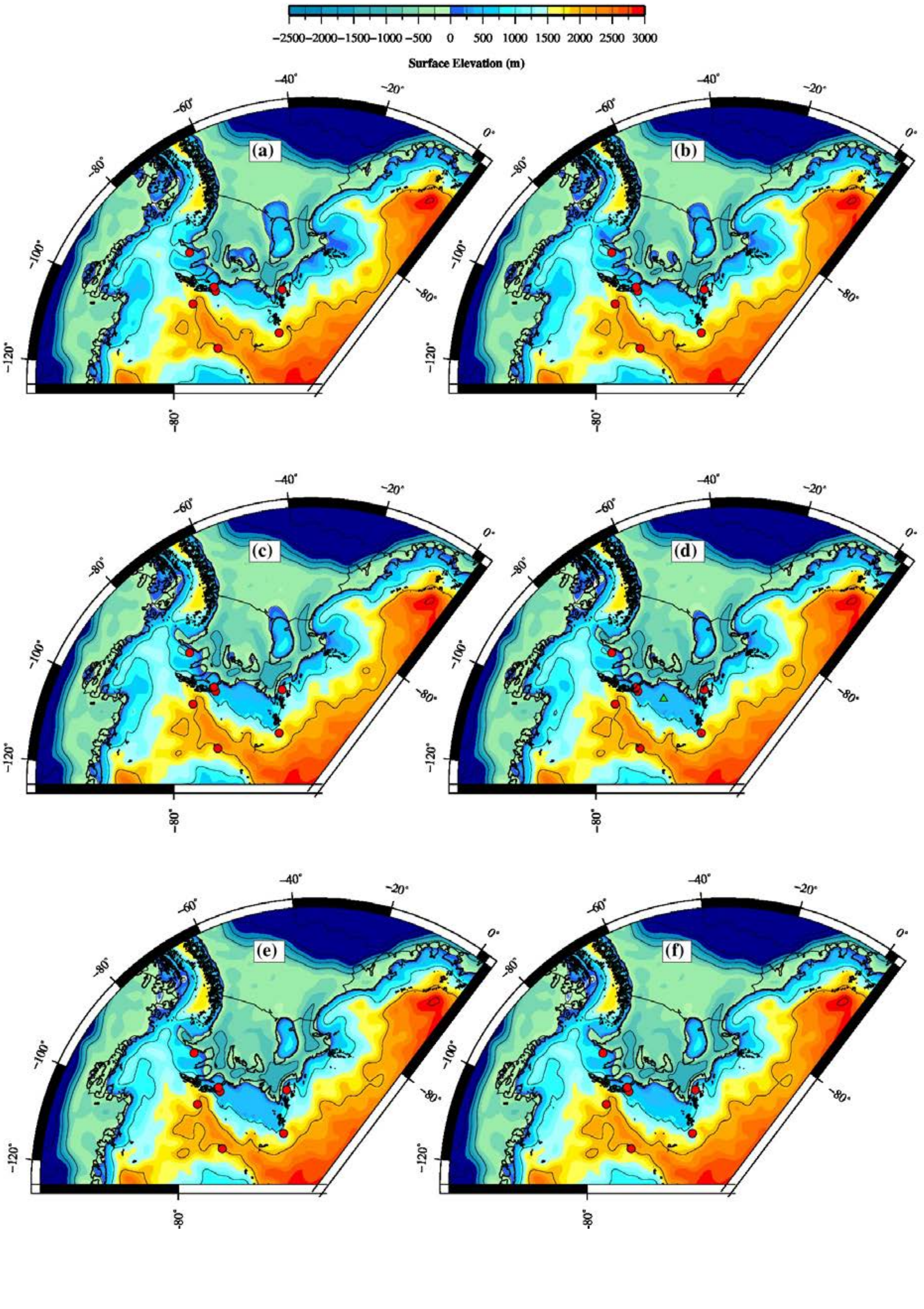

Fig. S2. Maps of surface elevation at a selection of times slices in the W12_Thin simulation: (a) 6 kyr BP, (b) 5 kyr BP, (c) 4 kyr BP, (d) 3 kyr BP, (e) 2 kyr BP and (f) 1 Kyr BP. The 0 kyr BP configuration for this model is identical to that shown in Fig. S1f. GPS sites are indicated by red circles, the location of the Robin Subglacial Basin is indicated by the green triangle in plot (d). Contours are drawn at 1000m intervals. Note that surface elevations greater than 3000 m are shown in red and bathymetry below -2500 m is shown in dark blue.

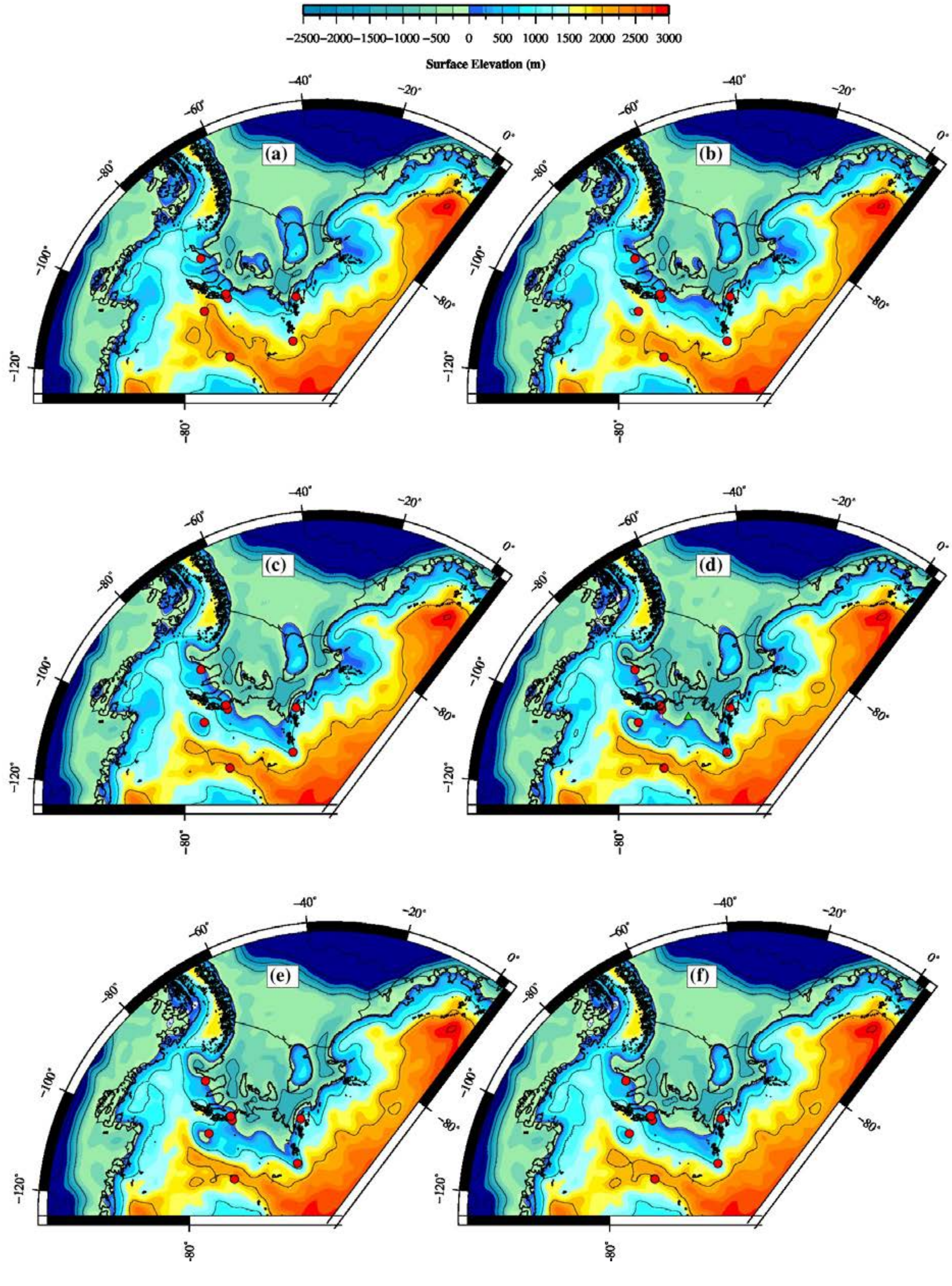

Fig. S3. Maps of surface elevation at a selection of times slices in the W12_Min simulation: (a) 6 kyr BP, (b) 5 kyr BP, (c) 4 kyr BP, (d) 3 kyr BP, (e) 2 kyr BP and (f) 1 Kyr BP. The 0 kyr BP configuration for this model is identical to that shown in Fig. S1f. GPS sites are indicated by red circles, the location of the Robin Subglacial Basin is indicated by the green triangle in plot (d). Contours are drawn at 1000 m intervals. Note that surface elevations greater than 3000 m are shown in red and bathymetry below -2500 m is shown in dark blue.

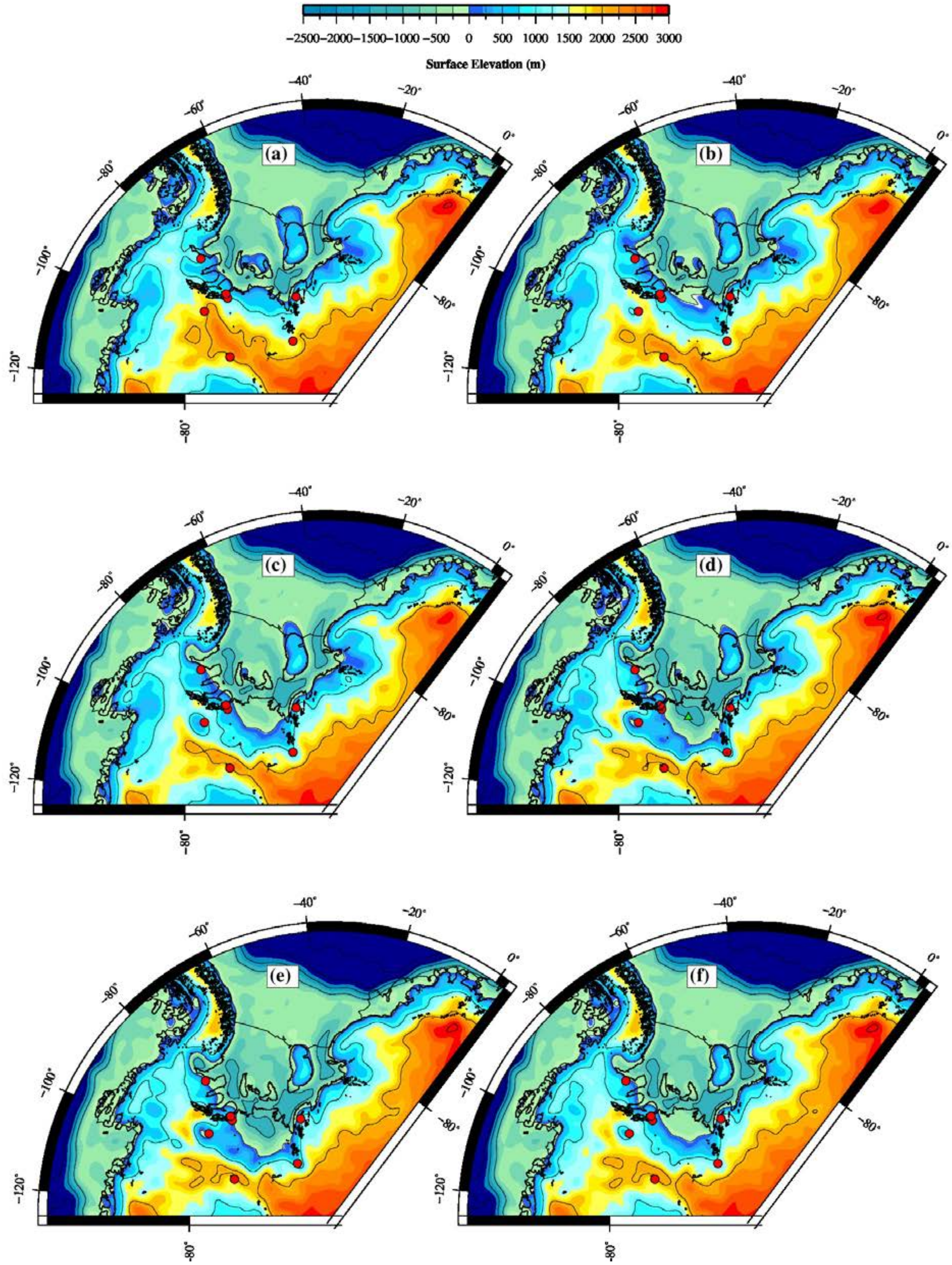

Fig. S4. Maps of surface elevation at a selection of times slices in the W12_Max simulation: (a) 6 kyr BP, (b) 5 kyr BP, (c) 4 kyr BP, (d) 3 kyr BP, (e) 2 kyr BP and (f) 1 Kyr BP. The 0 kyr BP configuration for this model is identical to that shown in Fig. S1f. GPS sites are indicated by red circles, the location of the Robin Subglacial Basin is indicated by the green triangle in plot (d). Contours are drawn at 1000m intervals. Note that surface elevations greater than 3000 m are shown in red and bathymetry below -2500 m is shown in dark blue.

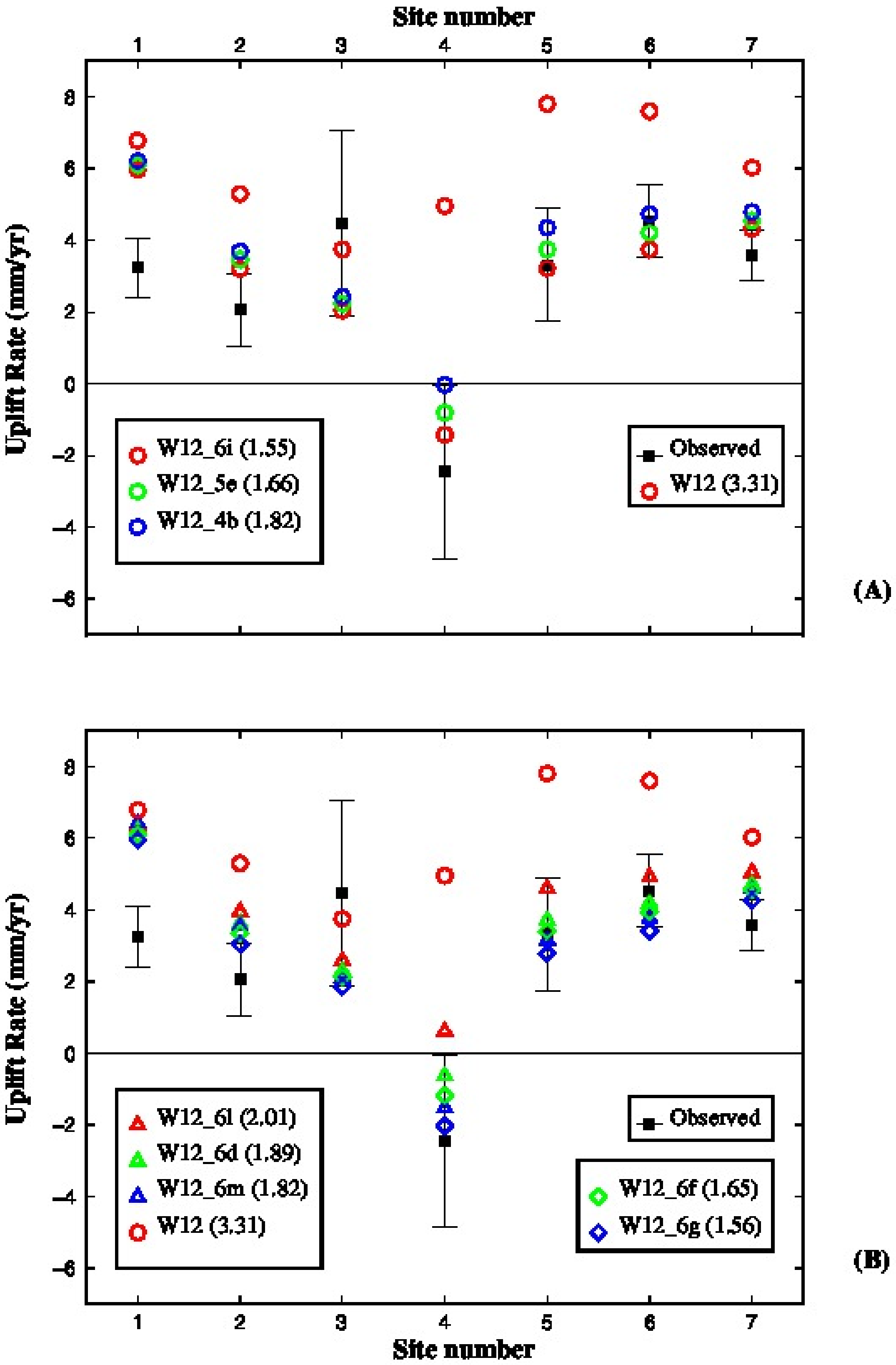

Fig.S5. Observed (elastic-corrected) (black squares, with1-sigma uncertainty) and modelled present-day uplift rates at the seven GPS sites, for a selection of the ice-loading simulations

(See Table 1 and text for more details) which compare changing the duration (kyr) and timing (kyr BP) of the retreat and readvance. An Earth model with a lithospheric thickness of 120 km and upper and lower mantle viscosities of 1×10^{21} Pa s and 1×10^{22} Pa s, respectively was adopted. The estimated WRMSE (mm/yr) for each simulation is given in brackets. (A) Comparison of ice-loading simulations with varying onset (kyr BP) and duration (kyr) of the simulated extended retreat from early (6 kyr BP) and long (3 kyr) retreat in W12_6i to short (1 kyr) and late (4 kyr BP) in W12_4b. (B) Comparison of ice-loading simulations with varying duration (kyr) and timing (kyr BP) for the end of the readvance from long (3 kyr) and late (0 kyr BP) in W12_6m, to short (1 kyr) and early (2 kyr BP) in W12_6l. The two sets of simulations compare different parameters for the retreat phase but the same duration (2 kyr) for the stillstand: W12_6l, W12_6d and W12_6m have a short (1 kyr) and early (6 kyr BP) retreat (6-5 kyr BP) and 2 kyr stillstand between 5-3 kyr BP; W12_6g and W12_6f have an early (6 kyr BP) 2 kyr retreat between 6-4 kyr BP, followed by a 2 kyr stillstand (4-2 kyr BP)

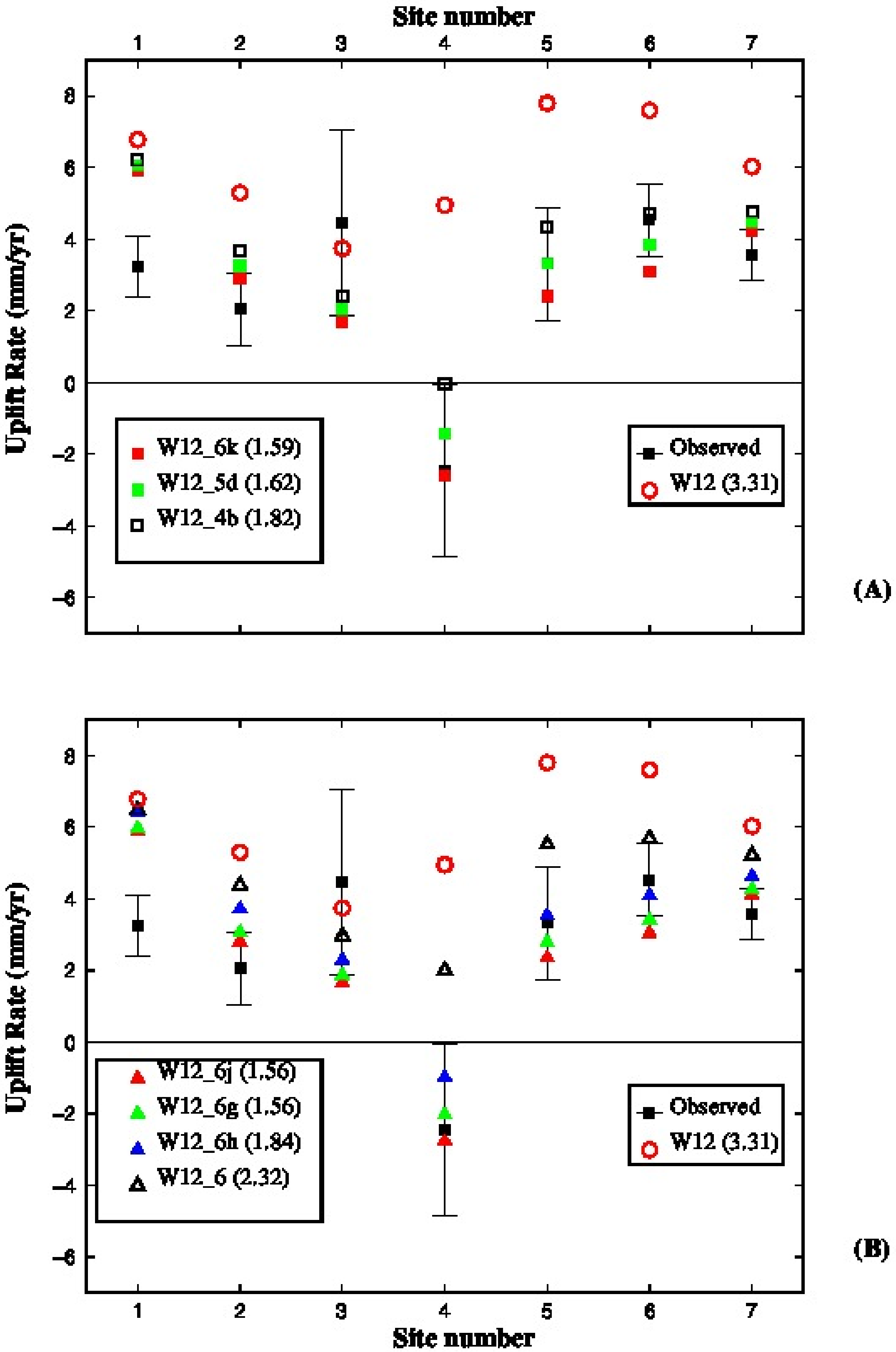
Site number
Uplift Rate (mm/yr)
W12_6k (1.59)
W12_5d (1.62)
W12_4b (1.82)
Observed
W12 (3.31)
(A)
W12_6j (1.56)
W12_6g (1.56)
W12_6h (1.84)
W12_6 (2.32)
Observed
W12 (3.31)
(B)
Site number

Fig.S6. Observed (elastic-corrected) (black squares, with 1-sigma uncertainty) and modelled present-day uplift rates at the seven GPS sites, for a selection of the ice-loading simulations that explore the sensitivity of predictions to the duration of the stillstand (see Table 1 and main text for more details) from 0 kyr, or no stillstand in W12, 1 kyr in W12_4b (A) and W12_6h (B), 2kyr in W12_5d (A) and W12_6g (B) and 3 kyr in W12_6k (A) and W12_6j (B) The estimated WRMSE (mm/yr) for each simulation is given in brackets.
(A) Comparison of ice-loading simulations with varying duration (kyr) and onset (kyr BP) of the extended retreat but constant readvance phase (2-0 kyr BP). (B) Comparison of ice-loading simulations with a constant retreat phase (6-4 kyr BP), but with varying duration of readvance.